論文 / 著書情報
Article / Book Information

題目(和文)	光線力学的治療応用に向けたGd2O3:Er,Ybアップコンバージョンナノ粒子の作製とその光学特性に関する研究
Title(English)	Study on preparation of Gd2O3:Er,Yb upconversion nanoparticles and their optical properties for photodynamic therapy
著者(和文)	鄭優莉
Author(English)	Yuri Tei
出典(和文)	学位:博士(工学), 学位授与機関:東京工業大学, 報告番号:甲第12771号, 授与年月日:2024年3月26日, 学位の種別:課程博士, 審査員:和田 裕之,北本 仁孝,曽根 正人,中村 健太郎,林 智広
Citation(English)	Degree:Doctor (Engineering), Conferring organization: Tokyo Institute of Technology, Report number:甲第12771号, Conferred date:2024/3/26, Degree Type:Course doctor, Examiner:,,,,
学位種別(和文)	博士論文
Type(English)	Doctoral Thesis

A doctoral dissertation

Study on preparation of Gd_2O_3:Er,Yb upconversion nanoparticles and their optical properties for photodynamic therapy

(光線力学的治療応用に向けた Gd_2O_3:Er,Yb アップコンバージョンナノ粒子の作製とその光学特性に関する研究)

Department of Chemical Science and Engineering,
School of Materials and Chemical Technology,
Tokyo Institute of Technology

Yuri Tei
February 2024

Supervised by
Associate Professor Hiroyuki Wada

List of Contents

Chapter 1
General introduction

1.1 Major cancer therapy and photodynamic therapy

It is well known that surgery, radiation therapy, and chemical therapy as a typical cancer treatments. Merit and demerit of those 3 typical cancer treatments are respectively. Surgery can enable us selective and physical removal of cancer tissue[1-1], however large burden is unavoidable on the patient's body. On the other hand, radiation therapy is no incision (non-invasive), but it also damages normal cells[1-2]. Chemical therapy is effective for a wide range of cancers that spread out, but it has strong side effect[1-3]. Therefore, the importance of non-invasive and selective destruction of cancer cells is raised. For example, as new cancer therapies, heavy ion radiotherapy and photodynamic therapy (PDT) have been developed nowadays.

Heavy ion radiotherapy is one of radiation therapy, that uses a carbon beam [1-4]. Used Heavy ions (carbon ions) accelerated to high speed. The merit of this therapy is deep inside cancer can be treated because radiation dose increases with depth, unlike X-ray which decreases with depth. Demerit of this therapy is that (1) large equipment & limited hospital (7 in Japan), and (2) restriction of target cancer as follow: ① solid cancer that stays in one area, ② not a recurrence of cancer, ③ no organs that move irregularly (stomach, large intestine)[1-5][1-6].

PDT uses photochemical reactions (Fig. 1-1). As a result, reactive oxygen species (ROS) that are generated from photosensitizers destroy cancer cells. ROS has cytotoxicity. The merit of PDT is ① first onset/recurrence cancer available, ② all primary malignant tumors, and ③ pinpoint treatment due to short-lived ROS (preservation of organ function)[1-7]. Demerit of PDT is superficial cancer is only treatable because visible light which is needed for photosensitizer activation is absorbed by the body[1-8][1-9]. The deep inside cancer and large volume cancer cannot be treated by current PDT. Therefore, expanding the treatment range of PDT is needed.

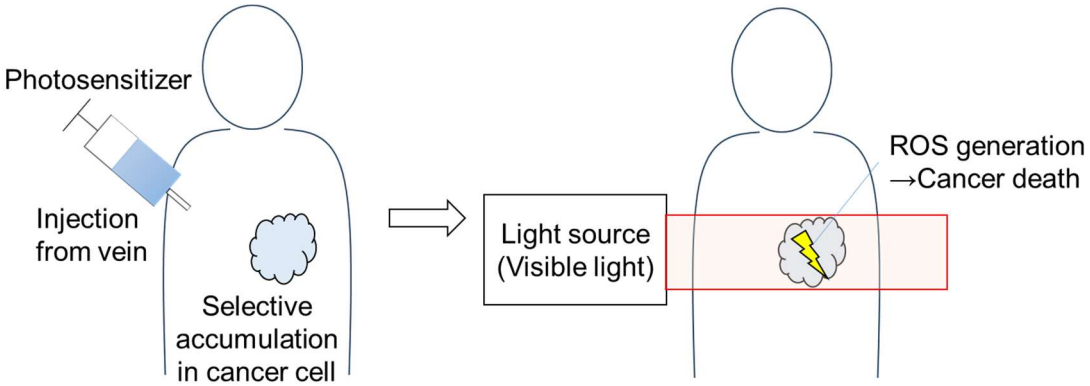

Fig. 1-1 PDT scheme.

1.2 Photodynamic therapy with upconversion nanoparticles

Since body tissue does not absorb near infrared light (NIR) which is within biological window[1-10]. Where visible light only reaches a few mm[1-11], NIR can reach a few cm deep from light irradiated surface[1-12] (Fig. 1-2).

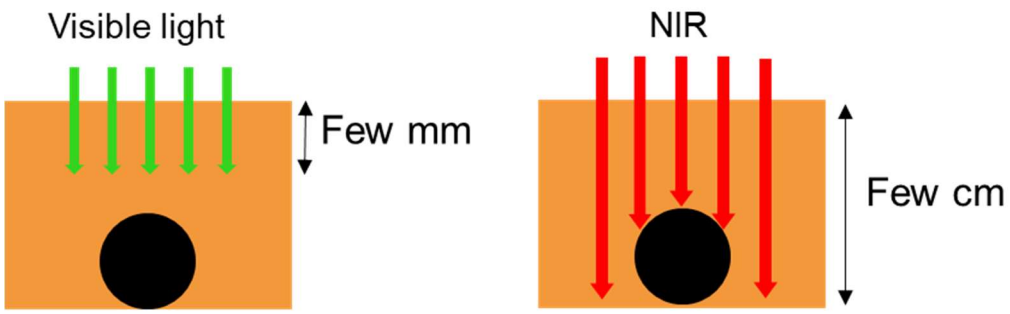

Fig. 1-2 Light penetration into the body.

Upconversion (UC) is the phenomenon in which longer wavelength light is converted to shorter wavelength light. If visible light can be obtained in cancer cells by UC from NIR which can reach deep inside, ROS will be also generated (Fig. 1-3). Applying NIR and UC nanoparticles (NPs) on PDT, the PDT treatment range will also be enlarged to deep inside cancer and large volume cancer too. In this study, UCNPs for PDT are investigated.

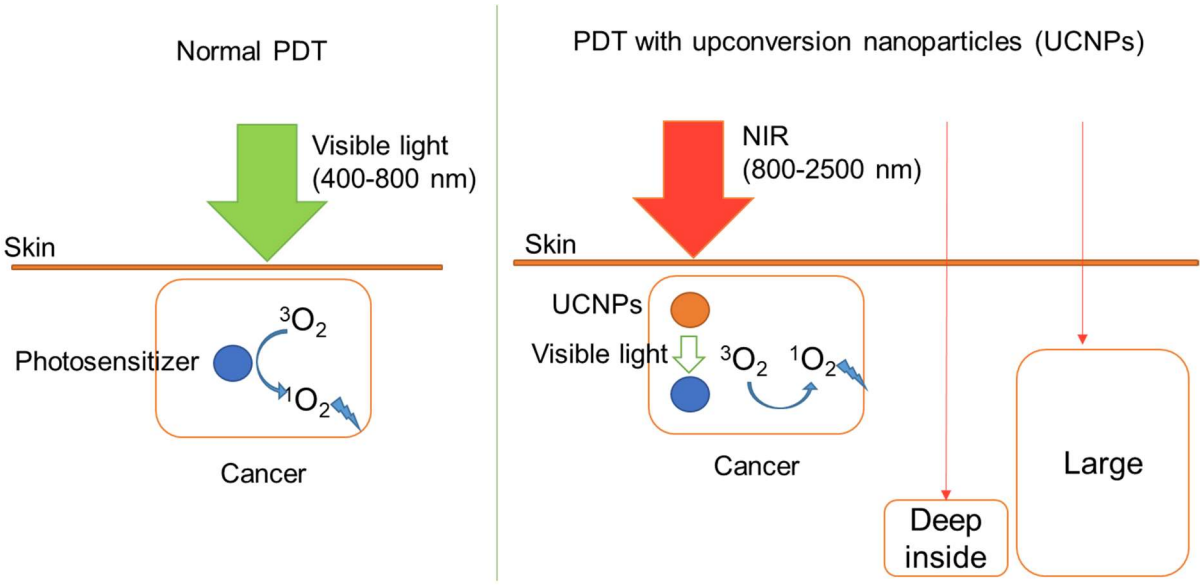

Fig. 1-3 Comparison of normal PDT and PDT with UCNPs.

1.3 Required condition for upconversion nanoparticles

Four tasks of UCNPs for PDT are shown in Tabel. 1-1.

Table. 1-1 Four tasks of UCNPs for PDT

Tasks	Detail	How to solve
① Excitation & emission range	・Excitation at 980 nm (NIR) ・Emission of visible light (400-800 nm)	←Yb (sensitizer) ←Er (activator)
② Emission intensity	・Correspondence of photosensitizer absorption area ・Prevention of energy loss (Low phonon energy material)	←Gd_2O_3 > $NaYF_4$ ←Gd_2O_3 > Y_2O_3
③ Particle size	・10-200 nm High crystallinity at first →Miniaturization maintaining high Crystallinity	Laser ablation in liquid
④Biocompatibility	Prevention of elimination from body as foreign matter	Surface coating with high biocompatibility material

(1) Excitation & emission range: It needs excitation at 980 nm NIR light and emission of visible light (400-800 nm). To solve this, optimal dopant ion selection is needed. This time, Yb ion (sensitizer) and Er ion (activator) were selected.

(2) Emission intensity: Upconverted visible light should have efficient light intensity at the corresponding wavelength of the photosensitizer's absorption area. It should have enough intensity to activate them. The strongest light emission area varied by changing the matrix. This time, Gd_2O_3 was selected for strong red light emission.

(3) Particle size: Since the UC phenomenon is needed in the cancer cell, it is needed to make them miniaturization (10-200 nm). Also, light emission intensity from phosphor depends on crystallinity, it is needed to maintain its crystallinity when miniaturization To solve this, laser ablation in liquid (LAL) is optimal.

(4) Biocompatibility: To prevent elimination by the body as a foreign matter after installation, surface coating around UCNPs with high biocompatibility material is needed.

The detailed solutions that correspond to each task in Table. 1-1 are described in next section 1.4.

1.4 Material condition setting for upconversion nanoparticles

1.4.1 Excitation and emission process (Yb, Er) [1-13]

In the case of UC materials based on inorganic crystals, the host material itself does not emit light (at room temperature). Therefore, UC luminescence can be obtained by doping a small amount of a luminescence ion in the matrix. The ions for light emission

are called “activators”, and the ions that provide energy to the activators are called “sensitizers”. UC emission can be obtained by carefully selecting the doping species and host material.

In this research, "excitation at 980 nm (NIR), emission of visible light (400-800 nm)" is required. And Er^{3+} (activator) and Yb^{3+} (sensitizer) are selected. The reason is shown below.

Since their 4f level, most lanthanide ions are capable of UC emission. In particular, Er^{3+}, Tm^{3+}, and Ho^{3+} have a band gap of $\Delta E = 10350\ (cm^{-1}) \rightarrow 966 \times 10^{-7}\ (cm) \rightarrow 966\ (nm)$, which means absorbing 970 nm (NIR) results in UC emission (Fig. 1-4 (Feng Wanga and Xiaogang Liu, 2009)[1-13]). Among them, Er^{3+} and Tm^{3+}, which have relatively large gaps between energy levels compared to Ho^{3+}, are effective as activators because their low tendency of energy loss (multiphonon relaxation). In this research, Er^{3+} which has energy levels that emit visible light ($^2H_{9/2}$ (blue), $^2H_{11/2}$, $^4S_{3/2}$ (green), and $^4F_{9/2}$ (red)) was selected as the activator.

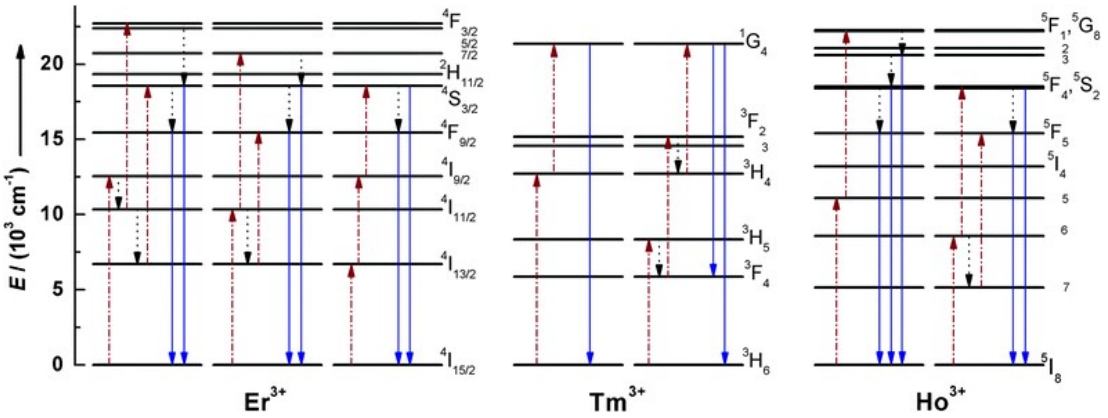

Fig. 1-4 Energy level of activator (Er^{3+}, Tm^{3+}, Ho^{3+})[1-13].

Most lanthanide ions have small absorption cross sections which means poor excitation efficiency from irradiation light. However, Yb^{3+}, which has only one excitation 4f level ($^2F_{5/2}$), has a larger absorption cross section than other lanthanide ions, and can efficiently donate energy by f-f transition with the activator Er^{3+} (Fig. 1-5 (Feng Wanga and Xiaogang Liu, 2009)[1-13]). Therefore, Yb^{3+} was selected as a sensitizer in this research.

Controlling the concentration of the activator and sensitizer is important because emission decrease (emission quenching) occurs if the doping ions are located too close to the host material or the activator concentration is too high. Thus controlling the concentration of sensitizer (~ 20 mol%) and activator (< 2 mol%) is also an important factor for UC emission.

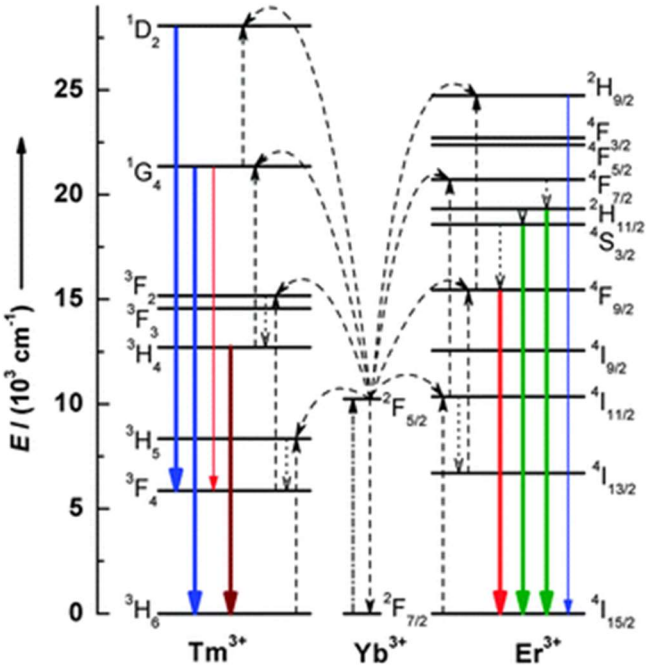

Fig. 1-5 One excited level of Yb^{3+} and efficient energy donation for activator [1-13].

1.4.2 Host material

Er and Yb can work when they dope in the host material. When selecting the host material, the following 2 parameters should be considered.

(1) Suitable material for photodynamic therapy

(2) Suitable material for UC

Details are described below.

(1) Suitable material for photodynamic therapy

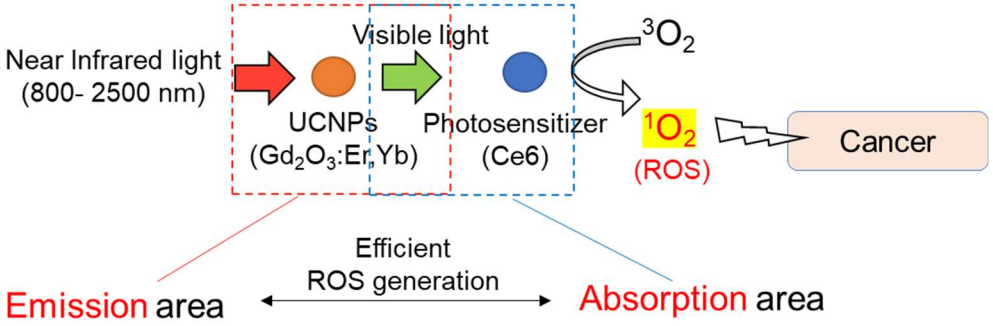

Fig. 1-6 Aiming PDT reaction scheme with UCNPs.

Fig. 1-6 shows the reaction scheme of PDT with UCNPs.

As shown in Fig. 1-6, the wavelength of upconverted light should correspond to the photosensitizer's absorption wavelength. Emission areas differ by type of host material even if the doping material is same.

As a photosensitizer for PDT, Chlorine e6 (Ce6) is suitable from the aspect of 8.8 times stronger absorption than typical photosensitizer Photofrin, quick elimination from the body, and high selectivity of cancer cells [1-14]. Ce6 has an absorption area of green (weak) and red (strong). Thus, to generate ROS, a strong red light is appropriate to activate Ce6.

Considering to obtain strong red light from UCNPs. As a phosphor, it is $NaYF_4$:Er,Yb is famous, however, their emission property is green > red emission. On the other hand, different host materials Gd_2O_3:Er,Yb have emission properties of green << red. Adding to it, hemoglobin absorbs < 600 nm where the green light is also included. $NaYF_4$ has a possibility of F desorption which is not an ideal condition for bio medical application. On the other hand, Gd_2O_3 is already used for MRI as one of the proven biological safety material and have high thermal and chemical stability[1-15].

Above all, Gd_2O_3:Er,Yb have appropriate emission area that corresponds to Ce6's strong absorption area and have biological safety. Thus, Gd_2O_3 is a suitable host material, especially for combination with PDT.

(2) Suitable material for UC emission

One of the phosphor materials, oxide can be a candidate[1-13]. As a former research, Nunokawa et al. reported Y_2O_3:Er,Yb[1-16][1-17]. As described in 1.4.1, the dopant is Er and Yb. As shown in Fig. 1-7, they exist at lanthanoid elements. For the property of phosphor, small lattice vibration is good for light emission. Lattice vibration is caused by each element that composes the crystal. Since the material characteristics are derived by electron movements within the crystal, when the lattice vibration is large, the electron's energy decreased by lattice vibration, resulting to luminescence inhibition. Lattice vibration increase when lattice strain large (Table. 1-2). However, lattice strain is unavoidable that dopant has always different radius with host material's. It is preferable that the similar radius of dopant and host material which result to small lattice strain.

From this point of view, lattice strain of Gd_2O_3 is smaller than Y_2O_3. To enhance component element of host material Gd_2O_3 will be suitable having similar radius with Er and Yb.

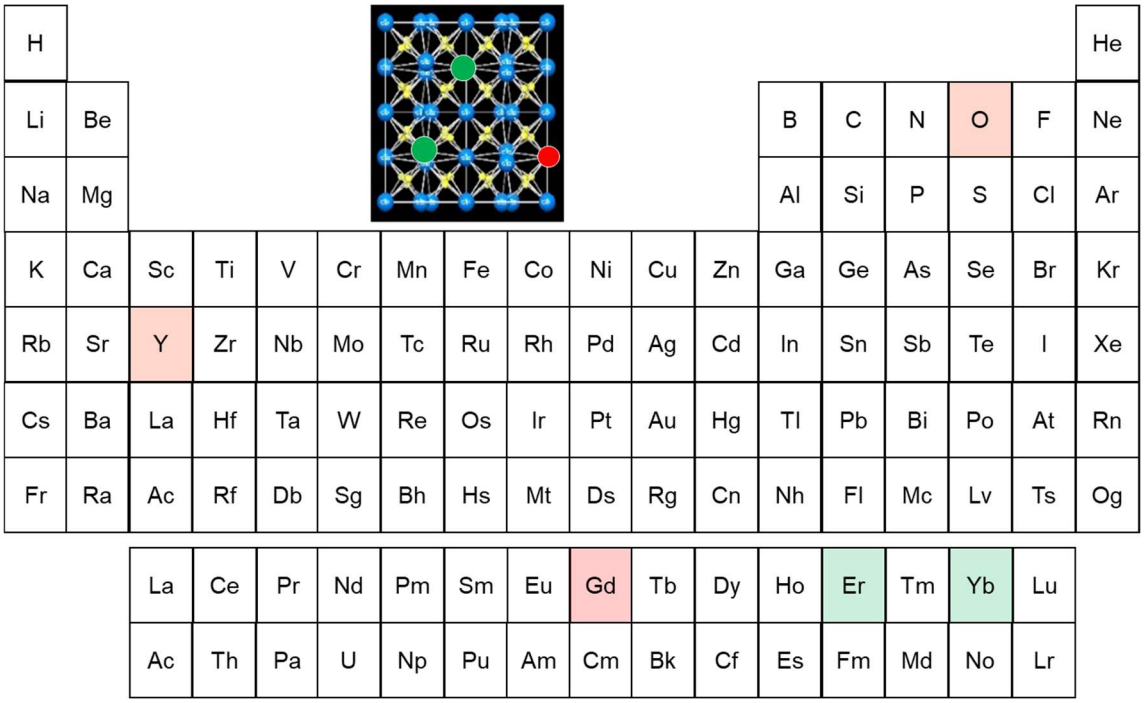

Fig. 1-7 Element of host material and doping material.

Table. 1-2 Qualitative comparison of host material

	Y_2O_3:Er,Yb	Gd_2O_3:Er,Yb
Lattice Strain	Large	Small
Lattice Vibration	Large	Small
Luminescence inhibition	Large	Small

From above 2 parameters (1) and (2), Gd_2O_3 is suitable for both PDT and luminescence.

1.4.3 Particle size

As shown in Fig.1-8, NPs can be selectively accumulated in cancer tissue by using enhanced permeability and retention (EPR) effect[1-18] and circulation in the body. Around cancer tissue, there is approx. 200 nm blood vessel gap which does not exist around normal cells. When NPs are circulating in the body after they are injected from vein, particle size < 200 nm NPs can be accumulated in cancer cells selectively. Elimination from the body occurs when the particle size is < 10 nm by the kidney[1-18] and >500 nm by the liver [1-19].

From the EPR effect and circulation in the body and elimination, the required particle size is 10-200 nm for selective accumulation.

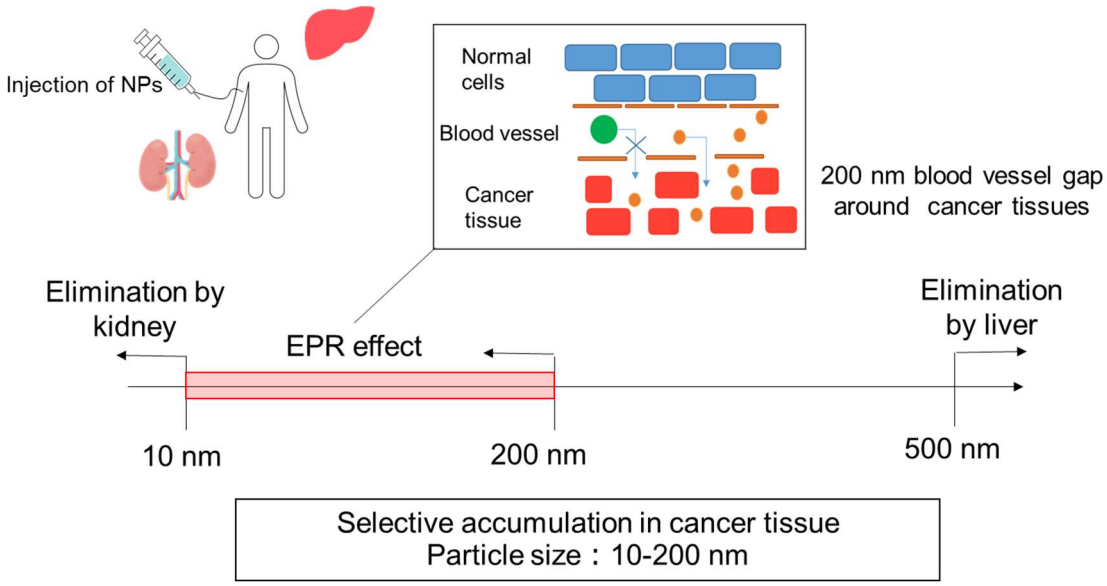

Fig. 1-8 Particle size for selective accumulation and elimination factor when circulating in the body.

1.4.4 Comparison of NPs fabrication method

Generally, the luminous efficiency of phosphor depends on synthesis temperature which results in high crystallinity [1-20]. High temperature avoids defects inside the crystal. Light emission is related to electron movement in crystal, defects prevent their movement by losing their energy.

Table. 1-3 shows a comparison of NPs fabrication method. As famous NPs fabrication method is solution method. It is possible to make smaller particles, but the synthesis temperature can be raised ~200℃ at most. Therefore, crystallinity and luminous properties are not enough for phosphor by solution method. Generally, for improving crystallinity, the phosphor is sintered at the latter process after gaining NPs. Sintering can improve crystallinity by heating at a temperature until < the melting point to adjust the crystal structure and remove internal strain (annealing). The higher the temperature, the higher the crystallinity [1-21]. However, the particles stick together each other in this process, so sintering is not sufficient from the aspect of "obtaining NPs". LAL is effective to get phosphor NPs which can miniaturizing raw materials maintaining its crystallinity. LAL can physically obtain NPs by laser irradiation onto a solid target placed in water. In addition, since it is no need to use reducing agents, it has the advantage for NPs for biomedical use [1-22]. Therefore, in this study, LAL was used for preparing phosphor NPs.

Table. 1-3 Comparison of NPs fabrication method

Method	Solution	Sintering	Laser ablation in liquid (LAL)
Temperature	~200℃	1200℃	Normal temp. in solution
			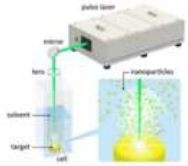 Physical conversion by laser Raw materials →NPs
Crystallinity	Low	High	High
Image of particle		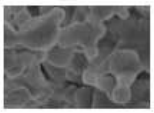	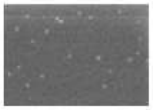
Particle size	○	×	○

1.5 Mechanism of laser ablation in liquid

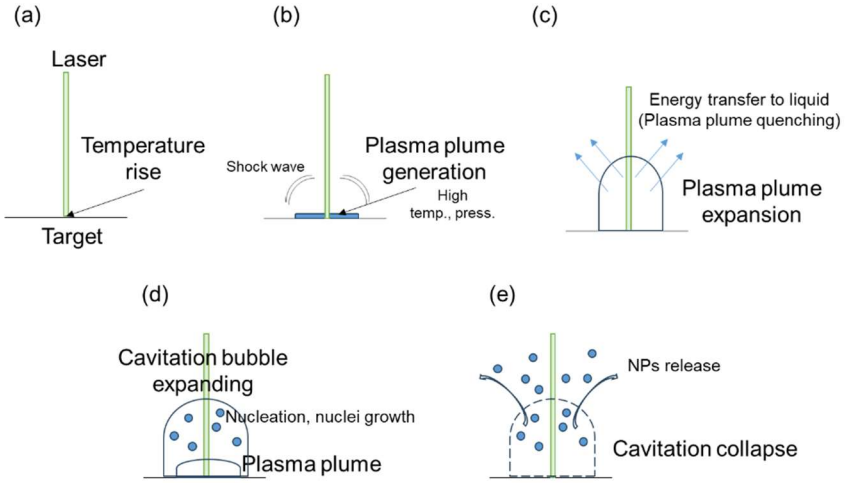

Fig. 1-9 Laser ablation in liquid mechanism (thermal evaporation mechanism).

LAL mechanism has not been completely clarified yet though, Fig. 1-9 shows one of the LAL mechanism[1-22]-[1-25]. Each process is explained below.

(a) Laser reaches the bulk, target absorbs the pulse laser. Energy from photons of laser transfer to the lattice and material temperature increase significantly.

(b) When the temperature exceeds the vaporization temperature, the material evaporates into the plasma plume generate on the surface (target-liquid). It includes ablated material; energetic species (atoms, molecules, ions, clusters, and dopants). The laser irradiated spot is high temperature and pressure. Accompanying to it, shock wave generate around there.

(c) By continuing laser absorption by bulk, ultrasonic adiabatic expansion of the plasma

plume occurs. However, the energy transfer of the plasma plume to liquid prevents more plasma plume expansion.
(d) During the expansion and cooling of the plasma plume, cavitation bubble occur. Also cavitation bubble expand to liquid. In this cavitation bubble, it is considered nucleation and nuclei growth occur.
(e) After the bubble reached to maximum size, it shrinked and collapsed results to NPs released to liquid.

This process is also called thermal evaporation mechanism[1-26]. Cavitation bubble inside condition has possibility the condition of temperature ~5000 K, pressure ~10^8 Pa, and heating and cooling rates >10^{10} K/s[1-27]-[1-29]. Therefore, it is considered nucleation and nuclei growth occur within the cavitation bubble.

1.6 Mechanism of laser melting in liquid [1-30][1-31]

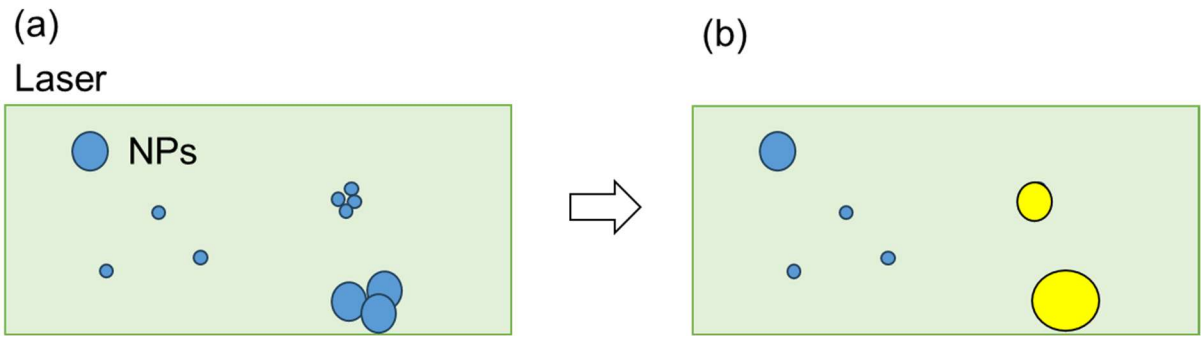

Fig. 1-10 Laser melting in liquid.

As shown in Fig. 1-10, pulsed laser melting in liquid (PLML) occurs at a low laser fluence (energy density: tens to hundreds of mJ/cm^2), and the light energy is converted into heat, causing heating, melting, evaporating of the particles. Therefore, the particle size of the product becomes larger than that of the original particle[1-30]- [1-32]. Although it is often performed with an unfocused laser, PLML can also occur with a focused laser depending on their condition[1-31].

1.7 Conditions for clinical application

The conditions to be considered for clinical application are: (1) immune reaction and biocompatibility, (2) NIR irradiation intensity, and (2) effect of NP shape.

1.7.1 Immune reaction and biocompatibility

Immunity is the function of protecting living organisms from attack and destruction from within the body (such as cancer) and outside the body (such as microorganisms). There are two types of immunity: defensive immunity (organs such as mucous membranes and skin prevent the invasion of microorganisms from outside) and offensive immunity (cells take in foreign substances that have entered the body and chemically destroy them (phagocytosis))[1-33].

Due to the action of the immune system, NPs may not reach the target site when they are introduced into the body. It has been reported that most non-surface-modified NPs are taken up by phagocytes[1-34]. In particular, biological reactions by NPs are caused by their surface properties[1-35]; It is effective to surface coating on the particle with a highly biocompatible material[1-35].

It is also reported that even if the same material of NPs, different biological behaviors are expressed depending on their conditions (surface coating, charge, size, hydrophobicity, solubility, shape, aggregation tendency, etc.)[1-34][1-35]. Therefore, NPs for biomedical use have the necessity of biocompatibility improvement and biological evaluation[1-35]. Biocompatibility evaluation is usually confirmed by the interaction between NPs and cells (*in vitro*)/ mice (*in vivo*).

As described above, NPs used in the body need to be biocompatible by surface coating, etc., for transporting them to the target site without immune reaction. It is also important to evaluate interactions and toxicity between NPs and biological specimens (such as bacteria and cells for first step of *in vitro* test).

1.7.2 NIR irradiation intensity

The maximum power density of NIR without damage to human skin tissue is 1 W/cm^2 [1-36]. On the other hand, the maximum power density of visible light is ~100-160 mW/cm^2[1-37][1-38]. NIR has a deep penetration depth and higher allowable maximum power density, therefore NIR is useful for clinical applications.

1.7.3 Effect of nanoparticle shape (fluorescence intensity/cancer accumulation)

It is known that when NPs are smaller than 100 nm, their chemical and physical properties change significantly compared to when they are larger[1-39]. One of these is improving the aggregation of NPs, but in this research, it is ideal to suppress of aggregation as much as possible and keep spherical shape as LAL fabricates. There are 3 reasons below.

Reason 1: It is related to fluorescence intensity. For the increase in fluorescence intensity, surface coating of surface defects on NPs is effective. However, if the NPs aggregate, the surface of the aggregated particles can be covered, but the areas where the particles touch each other (grain boundaries) cannot be covered. Because surface defects cannot be coated, the fluorescence intensity cannot be increased sufficiently. Furthermore, it has been reported that spherical phosphor NPs tend to have a stronger luminescence than irregular shapes[1-40].

Reason 2: Related to accumulation in organs. NPs smaller than 200 nm can accumulate in cancer tissues due to the EPR effect, but 10-100 nm size of NPs has higher accumulation rate in various cancer sites[1-41]. If agglomeration occurs, it is inappropriate because it may exceed the 10-100 nm size.

Reason 3: Shape-related. Disc-shaped particles have longer circulation times and higher accumulation, but spherical particles have faster cellular uptake when they bind to target cells[1-42]. By aggregating, it would be fine if the particles were to form disk-shaped of 10-100 nm, but since it is difficult to control to make them disc-shape successfully, aggregation is considered to be not suitable in this research.

As a countermeasure against aggregation, surface coating with a highly biocompatible material is effective.

1.8 Objectives of this study

The objectives of this study are to create NPs that meet the following conditions with the aim of expanding the treatment range of PDT, which is non-invasive and has less physical burden on patients compared to conventional, well-known cancer treatment methods.

(1) Fabrication of NPs by LAL while maintaining crystallinity

(2) Size of 10-200 nm NPs to prevent excretion from the body and selectively accumulate in cancer (EPR effect)

(3) Use NIR which has a larger maximum laser intensity for clinical use and deeper penetration depth than visible light.

(4) Converting NIR to visible light via UCNPs (use of Yb and Er as dopant). Especially, strong red emission corresponding to photosensitizer Ce6 (use of Gd_2O_3 as matrix)

(5) NPs surface coating aimed to improve biocompatibility, and fluorescence intensity, and keep single and spherical shape for high accumulation rate and uptake speed into cell

(6) Confirm the generation of ROS in the solution from the reaction scheme of PDT with

UCNPs

(7) Confirming the interaction between NPs and bacteria /cancer cells as a first step in biological application

1.9 References

[1-1] N. Onoda, S. Noda, S. Kashiwagi, K, Kurata, H. Kawajiri, T. Takashima, T. Ishikawa, and K. Hirakawa, Official J. Jpn. Assoc. Endocr. Surgeons Jpn Soc. Thyroid Surg., 30, (2013), 175.

[1-2] Y. Naoi and H Katayama, Juntendo Med. Journal (JMJ), 38, (1992), 30.

[1-3] S. Arawakawa, J. Jpn. Acad. Nurs. Sci., 16, (1996), 21.

[1-4] H. Kato, K. Kano, W. Anno, K. Tsuchida, Y. Takakusagi, N. Mizoguchi, I. Serizawa, T. Yoshida, and T. Kamada, J.Kyorin Med. Soc., 51, (2020), 133.

[1-5] M. Endo, Jpn. J. Med. Phys., 41, (2021), 10.

[1-6] K. Inafuku, H. Ito, M. Suzuki, T. Yokose, N. Nakayama, and M. Masuda, J. Jpn Assoc. Chest Surg., 32, (2018) 641.

[1-7] K. Hirakawa, S. Okazaki, H. Murakami, and N. Kanayama, JJSLSM, 41, (2021), 349.

[1-8] T. Yamamoto, H. Kozuki, T. Tsurubuchi, M. Matsuda, H. Akutsu, E. Ishikawa, S. Takano, and A. Matsumura, Jpn Neurosurg, 25, (2016), 905.

[1-9] Y. Nishiwaki, JJSLSM, 36, (2015), 138.

[1-10] S. Mallidi, G. P. Luke, and S. Emelianov, Trends Biotechnol., 29, (2011), 213.

[1-11] K. Soga, YAKUGAKU ZASSHI, 133, (2013), 355.

[1-12] T. Sato, Med. Photonics, 7, (2011), 53.

[1-13] F. Wanga and X. Liu, Chem. Soc. Rev., 38, (2009), 976.

[1-14] J. Minehisa, Y. Ii, A. Kaneda, and T. Yuzu, Oyo Buturi, 65 (1996) 31.

[1-15] P. Liu, F. Wang, and B. Yang, Solid State Sci., 102, (2020), 106165.

[1-16] T. Nunokawa, Y. Onodera, M. Hara, Y. Kitamoto, O. Odawara, and H. Wada, Appl. Surf. Sci., 261, (2012), 118.

[1-17] Y. Onodera, T. Nunokawa, O. Odawara, and H. Wada, J. Lumin., 137, (2013), 220.

[1-18] Y. Matsumura and H. Maeda, Cancer Res, 46, (1986), 6387.

[1-19] S. M. A. Sadat, S. T. Jahan, and A. Haddadi, J. Biomater. Nanobiotechnol. 7, (2016), 91.

[1-20] K. Y. Jung, C. H. Lee, and Y. C. Kang, Mater. Lett., 59, (2005), 2451.

[1-21] M. Yu, J. Lin, Z. Wang, J. Fu, S. Wang, H. J. Zhang, and Y. C. Han, Chem. Mater., 14, (2002), 2224.

[1-22] S. Hashimoto, Rev. Laser Eng., 45, (2017), 1.
[1-23] J. Liu , L. Huang, XM. Tian, XM Chen, YZ Shao, FK Xie, DH Chen, and L Li, Int. J. Nanomed., 12, (2017), 1.
[1-24] C. Lianwei and H. Minghui: “Laser Surface Structuring of Semiconductors and Functionalization” in Handbook of Laser Micro- and Nano-Engineering ed. by K. Sugioka, (Springer Nature, 2020) p.1.
[1-25] L. Chen, X. Jiang, Z. Guo, Hai Zhu, T. Kao, Q. Xu, G. Ho, and M. Hong, J. Nanomater., 2014, (2014), 1.
[1-26] H. Zeng, XW Du, S. C. Singh, S. A. Kulinich, S. Yang, and J. He, Adv. Func. Mater., 22, (2012), 1333.
[1-27] K. Sasaki, J. Plasma Fusion Res., 86, (2010), 324.
[1-28] Z. Yan, and D. B. Chrisey, J. Photochem. Photobiol. C, 13, (2012), 204.
[1-29] J. H. Bang and K. S. Suslick, Adv. Mater., 22 (2010), 1039.
[1-30] Y. Ishikawa, T. Tsuji, S. Sakaki, and N. Koshizaki, Prog. Mater. Sci. 131, (2023), 101004.
[1-31] N. Koshizakim, A. Pyantenko, H. Wang, and Y. Ishikawa, Rev. Laser Eng., 40, (2012), 83.
[1-32] A. Takami, H. Kurita, and S. Koda, J. Phys. Chem. B, 103, (1999), 1226.
[1-33] I. Nakajima, T. Takahashi, and T. Yoshikai: Simple meneki-gaku, (Nanko-do, 2017) p.3.
[1-34] S. Naahidi, M. Jafari, F. Edalat, K. Raymond, A. Khademhosseini, and P. Chen, J. Controlled Release, 166, (2013), 182.
[1-35] X. Li, L. Wang, Y. Fan, Q. Feng, and FZ. Cui, J. Nanomater., 2012, (2012), 548389.
[1-36] S. Lyu, Y. He, X. Tao, Y. Yao, X. Huang, Y. Ma, Z. Peng, Y. Ding, and Y. Wang, Nat. Commun., 13, (2022), 6596.
[1-37] S. Karrer, W. Bäumler, C. Abels, U. Hohenleutner, M. Landthaler, and RM. Szeimies, Lasers Surg. Med., 25, (1999), 51.
[1-38] G. B. Kharkwal, S. K. Sharma, Y. Huang, T. Dai, and M. R. Hamblin, Lasers Surg. Med., 43, (2011), 755.
[1-39] H. Kamiya and M. Iijima, The Micromeritics, 55, (2012) 12.
[1-40] K. Y. Jung, C. H. Lee, and Y. C. Kang, Mater. lett., 59, (2005) 2451.
[1-41] N. Khlebtsov and L. Dykmana, Chem. Soc. Rev., 40, (2011), 1647.
[1-42] A. S. Gupta, WIREs Nanomed. Nanobiotechnol., 8, (2016), 255.

Chapter 2
Effect of fluence and laser irradiation time on nanoparticles by laser ablation in liquid

2.1 Introduction

2.1.1 Fluence and laser irradiation time

LAL is a technology that causes laser ablation on solids in liquids and enables the production of various NPs[2-1]. As described in Chapter 1, since LAL's pulsed laser irradiation of raw materials is high energy, complex reactions occur under the conditions of high temperature, high pressure, and generation of plasma plume and cavitation bubble[2-2]. In particular, nucleation and nuclei growth of NPs are said to occur within cavitation bubbles. In LAL, various parameters (laser fluence, pulse width, beam diameter, laser wavelength, material composition, liquid type, surfactant usage) have a significant influence on the morphology, such as the size and shape of the NPs[2-3][2-4][2-5]. This is because they affect the absorption of laser energy, suppression of plasma plume expansion by liquid, and the maximum size and collapse time of cavitation bubbles. In particular, the size and collapse time of cavitation bubbles, where NPs are generated, are determined by the laser fluence[2-6]. Cavitation bubbles are considered to have a threshold value[2-7], the fluence was varied and investigated from which value LAL and NPs will occur. In addition, by extending the laser irradiation time, it is considered that the laser absorption by the material increases, and smaller NPs are generated[2-1].

Therefore, in Chapter 2, the fluence and the laser irradiation time were varied and their effects on NPs production, morphology and optical properties were investigated.

2.1.2 Classification

LAL tends to produce NPs with a wide size distribution due to the complex reaction mode and the large number of parameters[2-5]. In this study, size control is necessary from the perspective of PDT application. Classification is useful to obtain NPs solutions with narrow size distribution. Classification performs separation[2-8] using the difference in movement speed. There are roughly three types: (1) using gravity and centrifugal force applied to NPs (natural sedimentation, centrifugation), (2) using a stationary phase (chromatography, filter), and (3) using the charge of NPs in an electric field (requires machine, only in gas). Simple methods are centrifugation and filtering, but filtering has possibility to trap small particles too in the stationary phase.

Therefore, in Chapter 2, centrifugation was used to obtain a narrow size distribution of NPs.

2.2 Experimental

2.2.1 Preparation of target raw material Gd_2O_3:Er,Yb pellet

Since a focused laser is used for fabrication of NPs by LAL, target solid-state raw

material is needed. Target raw material Gd_2O_3:Er,Yb were made synthesized by sol-gel method and molded into pellet shape as following 4 steps (Fig. 2-1).

Used material were below: $Gd(NO_3)_3 \cdot 6H_2O$ (>99.95%, Kanto Chemical Co., Inc.), $Er(NO_3)_3 \cdot 5H_2O$ (>99.9%, Mitsuwa Chemical Co., Ltd), $Yb(NO_3)_3 \cdot 5H_2O$ (99.9% FUJIFILM Wako Pure Chemical Corporation), and aqueous ammonia (28%, Kanto Chemical Co., Inc.).

Step 1: Synthesis by sol-gel method

$Gd(NO_3)_3 \cdot 6H_2O$ (5.020 g, 89.0 mol%), $Er(NO_3)_3 \cdot 5H_2O$ (0.0554 g, 1.00 mol%), and $Yb(NO_3)_3 \cdot 5H_2O$ (0.5614 g, 10.0 mol%) were measured by precision electronic balance. They were completely dissolved in pure water (50 mL) of plastic beaker after ultrasonication for 30 min (ASONE, ASU-2). pH paper showed the solution was alkaline. Aqueous ammonia (11 mL) was added by drop while stirring by stirrer at 250 rpm. After stirring continued for 2 hours, the solution was aged for 24 hours without stirring. Here, white precipitate of desired material Gd_2O_3:Er,Yb was synthesized by sol-gel method.

Step 2: Separation and drying

To separate the white precipitate from the liquid, the precipitate and the original solution liquid were poured into 2 of 50 mL plastic centrifugation tubes, and centrifugated at 5000 rpm for 10 min (ASONE, CN-1050). Super tenant solution was poured out and pure water was added to wash and centrifugated at 5000 rpm for 10 min. This washing process was repeated 3 times. The washed white precipitate on the evaporating dish was dried by vacuum drying (AS ONE, AVD-250V) for 12 hours. Here dried white powder was obtained.

Step 3: Firing

The dried white powder in a crucible was fired in an electric furnace (Nitto Kagaku Co., ltd., NHK-170) at 900℃ for 2 hours (heating rate: 300℃/hour, natural cooling rate: 600℃/hour).

Step 4: Pellet molding and sintering

After the fired white powder was grinded by mortal for 10 min, approximately 0.8 g of powder was molded into pellet shape as d= 9.5 mm, pressed at ~140 MPa for 5 min by press equipment (TOKYO HYDRAULIC EQUIPMENT, ESE-077-00). The molded pellet was placed in a boat-shaped crucible, sintered in the electric furnace at 1200℃ for 2 hours (heating rate: 300℃/hour, natural cooling rate: 600℃/hour). Pellet thickness was

around 2.5 mm. Here, the desired raw material Gd_2O_3:Er,Yb pellet was obtained (Fig. 2-2).

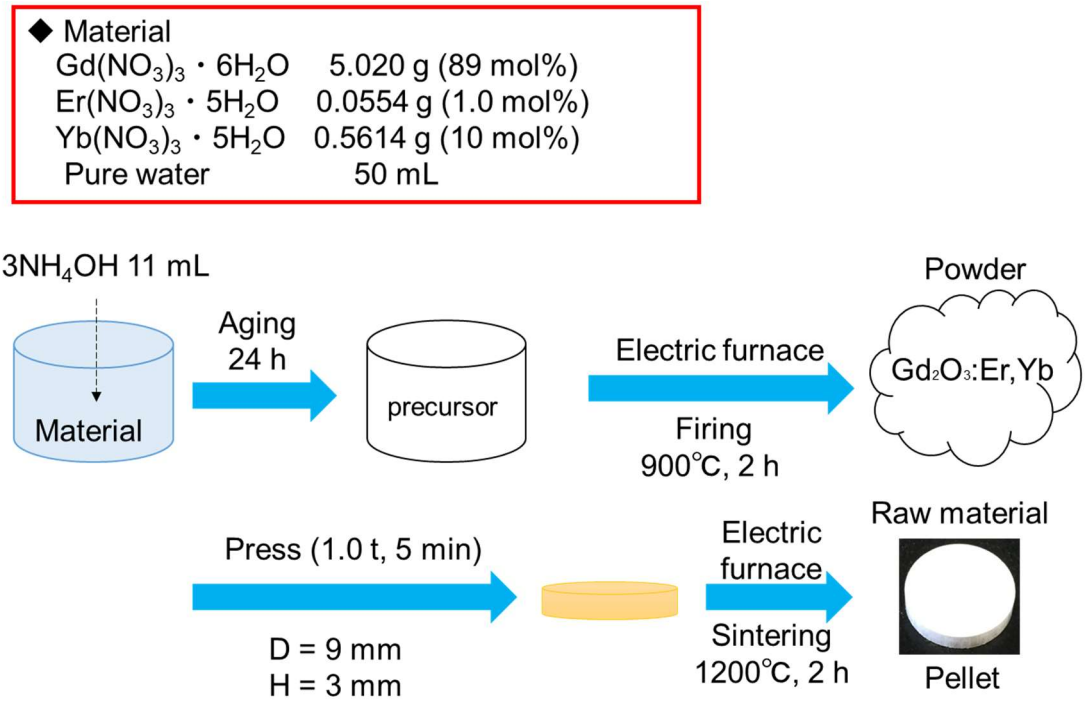

Fig. 2-1 Raw material preparing procedure.

Fig. 2-2 Prepared Gd_2O_3:Er,Yb pellet.

2.2.2 Laser equipment for LAL

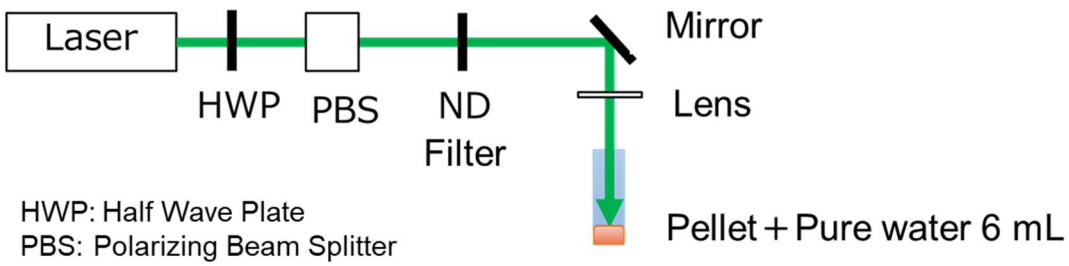

Fig. 2-3 Laser equipment for LAL.

Fig. 2-3 shows schematic of the used laser equipment for LAL. As a light source of laser, Nd:YAG laser with second harmonic generation to a wavelength of 532 nm; repetition frequency was 10 Hz, the pulse width was 13 ns, and the laser was focused onto the target material through a focusing lens. Target pellet was placed in 6 mL water in 30 mL bin.

Using this equipment, following were studied;

- Effect of laser intensity (fluence) on NPs by LAL
- Effect of laser irradiation time on NPs by LAL
- Classification by centrifugation

The detailed procedure of 3 experimental and characterization are explained from at sections 2.2.3, 2.2.4, and 2.2.5 for each.

2.2.3 Effect of laser intensity (fluence) on NPs by LAL

2.2.3.1 Preparation of NPs and laser condition

As an investigation of fluence effect on NPs by LAL, the same equipment as Fig. 2-3 was used. Fluence was varied from 2.4, 4.7, 6.4, 8.7-8.9 J/cm^2, and laser irradiation time was 30 min for each. Obtained NPs solution was characterized as follows.

2.2.3.2 Characterization

(1) Element analysis by Transmission Electron Microscope and Energy Dispersive Spectroscopy (TEM-EDS)

Element analysis of both obtained NPs and the raw material were measured by TEM-EDS (FE-TEM (JEOL, JEM-2100F)- EDS (JEOL, JED-2300T)). The accelerating voltage of TEM was 200kV. TEM grid with a collodion membrane was used. The measurement sample was prepared as follows.

-The raw material sample: The raw material pellet was crushed with a cutter to obtain fragments, and then ground in a mortar.

- NPs sample: Obtained NPs solution at 8.7 J/cm^2 in plastic tube was frozen and freeze dried by a freeze dryer (EYELA, FDU-120). The same cycle was repeated until the amount of powder became sufficient.

(2) Crystal structure analysis by X-ray diffraction (XRD)

Crystal structure analysis of both the raw material and obtained NPs were measured by XRD (Rigaku, Ultima IV). XRD analysis condition was 2θ=20-80°, Cu tube. The measurement sample was prepared as follows.

-The raw material sample: The raw material pellet was crushed with a cutter to obtain

fragments, and then ground in a mortar.

- NPs sample: Obtained NPs solution at 6.4, 8.7 J/cm^2 in plastic tube was frozen and freeze dried by a freeze dryer (EYELA, FDU-120). Obtained powder is not sufficient for XRD analysis if it is only a one-time LAL, the same cycle was repeated until the amount of powder became sufficient.

(3) Morphology and primary particle size analysis by Scanning Electron Microscope (SEM)

Morphology and primary particle size analysis of both the raw material and obtained NPs were observed by SEM (Hitachi High technologies, S-4800). Observation samples were prepared as follows.

- The raw material sample: The raw material pellet was crushed with a cutter and the pieces were placed on carbon tape.
- NPs samples: Approximately 50 μL supernatant of the obtained solution at each fluence was dried on Cu grid (Okenshoji Co., Ltd., elastic carbon membrane, ELS-C10).

The observation was performed while filling with liquid nitrogen in the SEM body for the clear SEM images.

(4) Secondary particle size measurement by Dynamic Light Scattering (DLS)

Secondary particle size analysis of the obtained NPs at each fluence was measured by DLS (Sysmex Co, Zetasizer Nano). Measurement sample was poured in plastic cell from 1 mL supernatant of obtained NPs solution at each fluence.

(5) Photoluminescence measurement by photoluminescence spectrometer (PL)

Photoluminescence intensity of obtained NPs solution was measured by PL (HITACHI, F-7000). Light source was composed of laser diode (THORLABS, L980P300J), laser mount (HORLABS, TCLDM9), and temperature and current controller (THORLABS, LTC100 B). Measurement condition was excitation wavelength 980 nm, photomultiplier voltage 700 V, slit 1.0 nm, monitoring wavelength 400-800 nm.

Measurement sample was poured in quartz cell from 1 mL supernatant of obtained NPs solution at each fluence.

(6) Photon number measurement by PL

The photon number for light emission was measured by PL same equipment as 2.2.3.2.(5). Measurement condition was excitation wavelength 980 nm, photomultiplier

voltage 700 V, slit 1.0 nm, monitoring wavelength 400-800 nm.

Measurement sample was poured in quartz cell from 1 mL supernatant of obtained NPs solution at each fluence. The fluorescence intensity value was measured while varying the input current value.

2.2.4 Effect of laser irradiation time on NPs by LAL

2.2.4.1 Preparation of NPs and laser condition

As a investigation of laser irradiation time effect on NPs, the same equipment as Fig. 2-3 was used. Fluence was set at one fluence (5.7 J/cm^2), and laser irradiation time was varied 5, 15, and 30 min. Obtained NPs solution was characterized as follows.

2.2.4.2 Characterization

(1) Morphology and primary particle size analysis by SEM

Morphology and primary particle size analysis of obtained NPs observed by the same SEM equipment as 2.2.3.2.(3). Preparation method of observation NPs samples at each laser irradiation time were prepared as same procedure as 2.2.3.2.(3). The observation was performed while filling the SEM body with liquid nitrogen for the clear SEM images.

(2) Secondary particle size measurement by DLS

Secondary particle size analysis of the obtained NPs at each laser irradiation time was measured by the same DLS as 2.2.3.2.(4). Preparation method of measurement NPs samples at each laser irradiation time were prepared as same procedure as 2.2.3.2.(4).

(3) Photoluminescence measurement by PL

Photoluminescence intensity of obtained NPs solution was measured by the same PL as 2.2.3.2.(5). Measurement condition was excitation wavelength 980 nm, photomultiplier voltage 700 V, slit 2.5 nm, monitoring wavelength 400-800 nm.

Measurement sample at each laser irradiation time were prepared as the same procedure as 2.2.3.2.(5).

(4) Photon number measurement by PL

The photon number for light emission was measured by PL same equipment as 2.2.3.2.(5). Measurement condition was excitation wavelength 980 nm, photomultiplier voltage 700 V, slit 2.5 nm, monitoring wavelength 400-800 nm.

Measurement sample at each laser irradiation time were prepared as same procedure as 2.2.3.2.(6). Fluorescence intensity value was measured while varying the input current

value.

(5) Zeta potential by DLS

Zeta potential of the obtained NPs was measured by the same DLS as 2.2.3.2.(4) Measurement sample was poured in the capillary zeta cell (Malvern, DT1070) from 700μL supernatant of obtained NPs solution at each irradiation time.

2.2.5 Classification by centrifugation

2.2.5.1 Preparation of NPs and laser condition

NPs sample was fabricated by same laser equipment as Fig. 2-3. Fluence was set at one fluence (9.0 J/cm^2), and laser irradiation time was 15 min. All of the NPs solution (6 mL) were centrifugated (5000 rpm × 20 min) for particle classification. The centrifugated solution was separated by 1 mL from top and each layer was measured by PL. After that, each layer of solution was vacuum dried. The sample were re-dispersed in 1 mL water for each for SEM observation.

2.2.5.2 Characterization

(1) Photoluminescence measurement by PL

Photoluminescence intensity of obtained NPs solution was measured by the same PL as 2.2.3.2.(5). Measurement condition was excitation wavelength 980 nm, photomultiplier voltage 700 V, slit 2.5 nm, monitoring wavelength 400-800 nm.

Measurement sample at each laser irradiation time were prepared as same procedure as 2.2.3.2.(5).

(2) Morphology and primary particle size analysis by SEM

Morphology and primary particle size analysis of obtained NPs observed by the same SEM equipment as 2.2.3.2.(3). Preparation method of observation NPs samples at each laser irradiation time were same procedure as 2.2.3.2.(3). The observation was performed while filling liquid nitrogen in the SEM body for the clear SEM images.

2.3 Results and discussion

2.3.1 Effect of laser intensity (fluence) on NPs by LAL[2-9]

2.3.1.1 Element analysis by TEM-EDS

Fig. 2-4 shows TEM-EDS element analysis results of (a) raw material and (b) NPs (8.7 J/cm^2) by LAL. In both results of (a) raw material and (b) NPs by LAL, O, Gd, and Yb were observed as their components. Regarding Er, it was same peak at Gd, Yb and doping

concentration was too low, therefore Er could not observed in these results. However, from Fig. 2-4, it is considered that the host material is composed by Gd and O, and Yb was doped into host material by the assuming reaction (sol-gel method). Adding to it, it was clarified NPs by LAL maintained their original raw material's components.

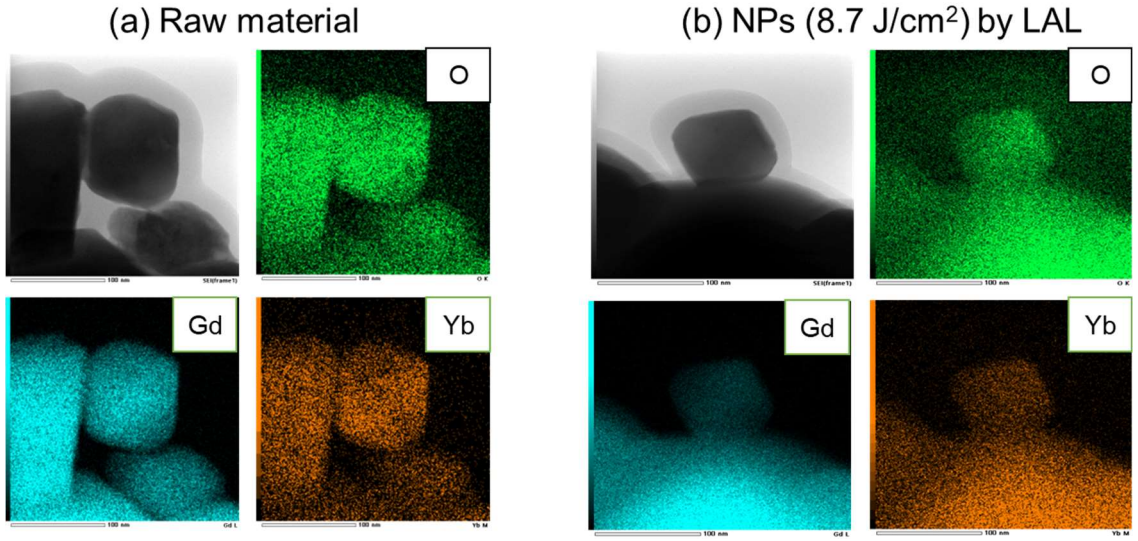

Fig. 2-4 TEM-EDS element analysis of (a) raw material and (b) NPs (8.7 J/cm^2) by LAL.

2.3.1.2 Crystal Structure by XRD

Fig. 2-5 shows crystal structure analysis result by XRD. The peaks of the NPs and raw materials were identified based on the standard data of the Powder Diffraction File: cubic Gd_2O_3 (# 00-012-0797), and monoclinic Gd_2O_3 (# 00-043-1015). Peaks were from cubic and monoclinic of Gd_2O_3. All peaks from NPs and raw materials appeared at same degree, had no other peaks than Gd_2O_3. From these results, the crystal structure of obtained NPs was not changed from raw material's due to laser irradiation, and no by-products generated.

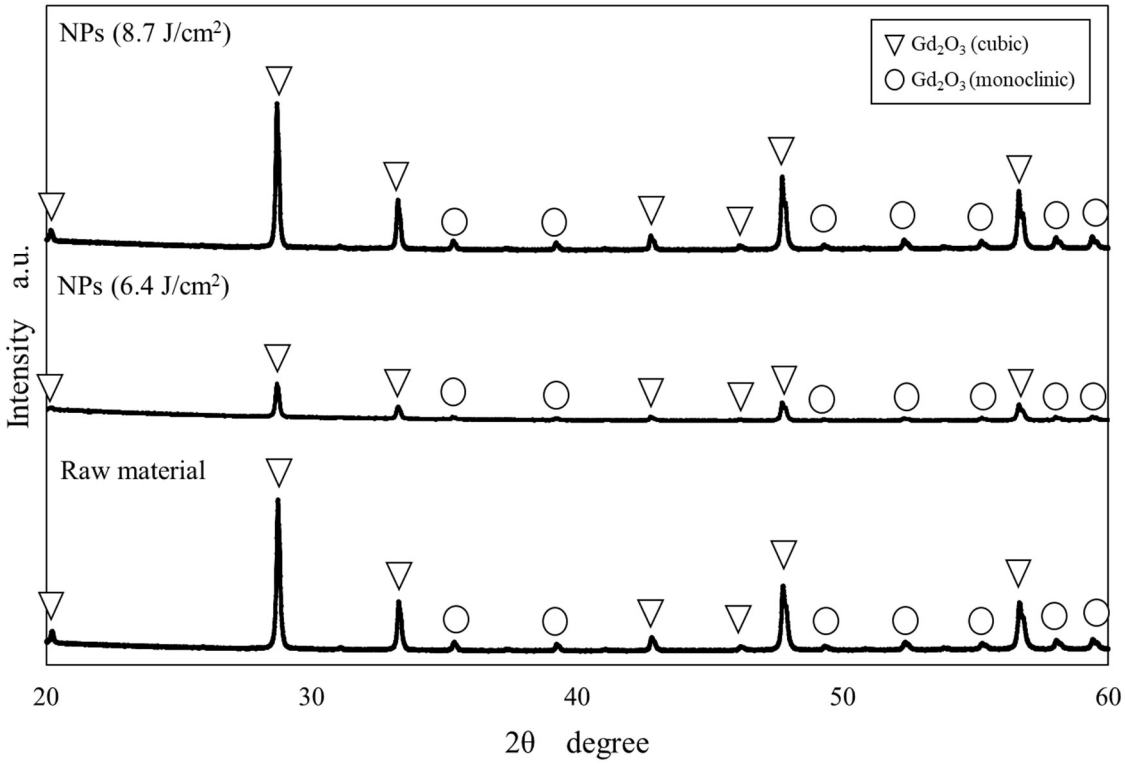

Fig. 2-5 Crystal structure of NPs (6.4, 8.7 J/cm^2) and raw material.

2.3.1.3 Primary particle size by SEM and distribution

Each grain size corresponds to the primary particle size, whole particle size corresponds to the secondary particle size if it's composed by several grains.

Fig. 2-6 shows the results of the primary particle size observation by SEM. Fig. 2-6 (a) shows raw material, and Figs. 2-6 (b)–(g) shows the NPs after laser irradiation. The primary particle size of raw material in Fig.2-6 (a) was ~200-300 nm, each particle is different in shape and condensed each other because of sintering process. After laser irradiation, the following was observed; Coarse NPs whose primary particle size was 200-300 nm at low fluence (~2-5 J/cm^2) in Figs. 2-6 (b) and (c), coarse NPs and below 100 nm sized fine NPs at the middle fluence (~6 J/cm^2) in Figs. 2-6 (d) and (f), increased fine NPs at the high fluence (~9 J/cm^2) in Figs. 2-6 (e) and (g).

Since the primary particle size of coarse NPs was similar to raw material's at low fluence, coarse NPs were generated due to the shock of laser hitting the raw material (fragmentation). Or the possibility of PLML, by hitting the low fluence laser to particles which locate near site because laser is Gaussian distribution. Lasers follow a Gaussian distribution, therefore 90% of the energy is concentrated near the center of the laser beam (within a radius of less than 30%)[2-10], and the fluence is weaker outside of center.

On the other hand, fine NPs were smaller than raw material's primary particle size, therefore it is not generated by fragmentation but by the LAL process (thermal evaporation mechanism; refer to section 1.5). As described in section 2.1.1, at high fluence, cavitation bubble expanded with fluence increase, nucleation and nuclei growth occurred inside of it, and NPs generated. Adding to it, middle fluence is considered to beyond threshold of LAL. But it is not a large cavitation bubble (firster collapse time) compared to high fluence's, therefore small number of fine NPs were obtained.

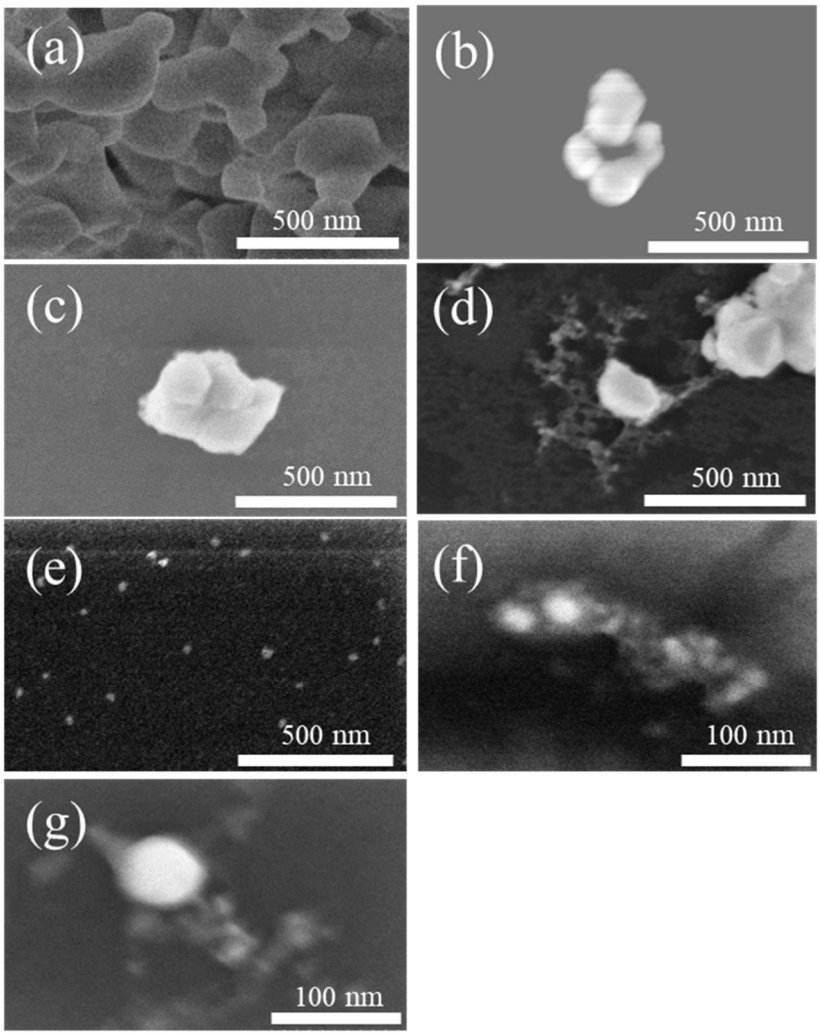

Fig. 2-6 SEM images of (a) raw material, the generated particles at (b) 2.4 J/cm^2, (c) 4.7 J/cm^2, (d) 6.4 J/cm^2, (e) 8.9 J/cm^2, (f) fine NPs at 6.4 J/cm^2, and (g) fine NPs at 8.9 J/cm^2.

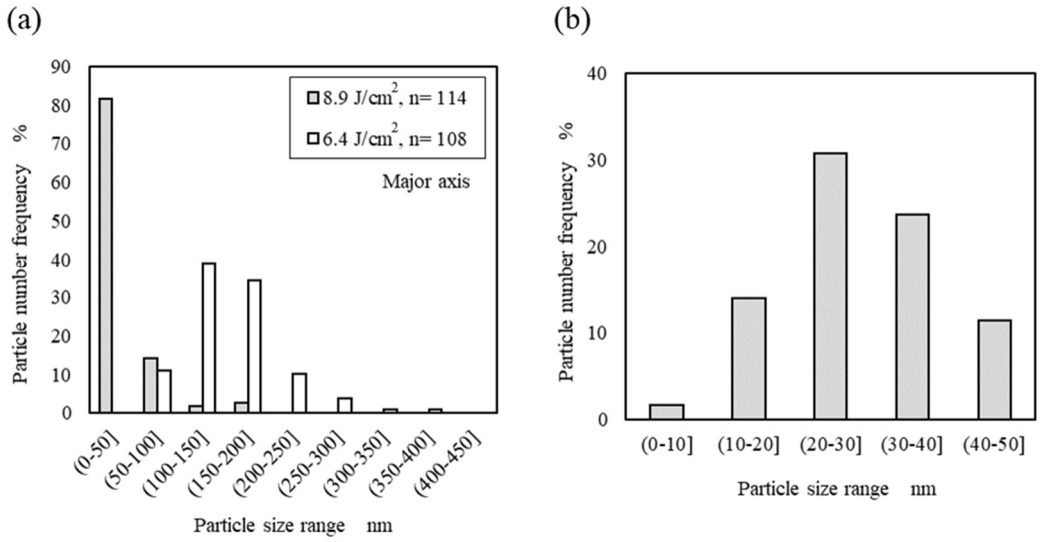

Fig. 2-7 Primary size histogram of (a) NPs at middle and high fluence and (b) NPs at a high fluence in the range of 0-50 nm.

Fig. 2-7 shows primary particle size distribution changing by the data of NPs at middle and high fluence. Fig. 2-7 (a) shows results of all, Fig. 2-7 (b) shows the detail data within 50 nm of high fluence data. From Fig. 2-7 (a), at middle fluence, 100-200 nm was majority, and < 100 nm fine NPs were started to generate. At high fluence, distribution shifted to the left, increasing fine NPs. Especially within 50 nm in Fig.2-7 (b), primary particle size 0-10 nm was 1.8 % which will be eliminated by kidney. However, most of this Fig. 2-7 (b) won't be eliminated. From these results, the NPs range of 10-200 nm which is needed for PDT can be fabricated at middle and high fluence under 30 min laser irradiation.

2.3.1.4 Secondary particle size by DLS

As shown in Fig. 2-8, the secondary particle size at each fluence was measured by DLS. From Fig. 2-8 (a), particle size distribution was unimodal. Compared to the distribution of low fluence, left shoulder width increased at middle fluence, and both shoulder widths increased at high fluence. Mode secondary particle size was picked up in Fig. 2-8 (b), and it was within the range of 250-350 nm at each fluence. Regarding the result at high fluence, the mode secondary size was larger than the primary particle size of SEM.

The cause is considered by 2 points of view; (1) grain gradient: used liquid volume was only within 100 μL of supernatant for SEM, but 1 mL of supernatant is needed for DLS which may allow to include coarse NPs which exists lower layer of bin (generated by fragmentation or PLML due to weak part of gaussian distribution), (2) aggregation of fine NPs. Aggregation possibility increases as the number of the particle increases at high

fluence due to its increased collision frequency. The other consideration for aggregation is the lower surface potential of decreased particle size.

(a) Secondary particle size distribution

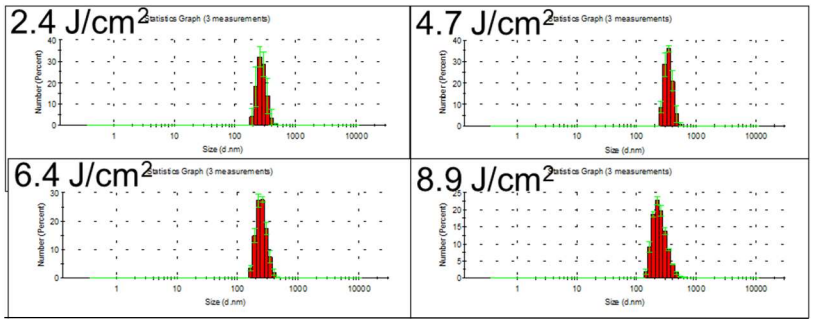

(b) Mode secondary particle size

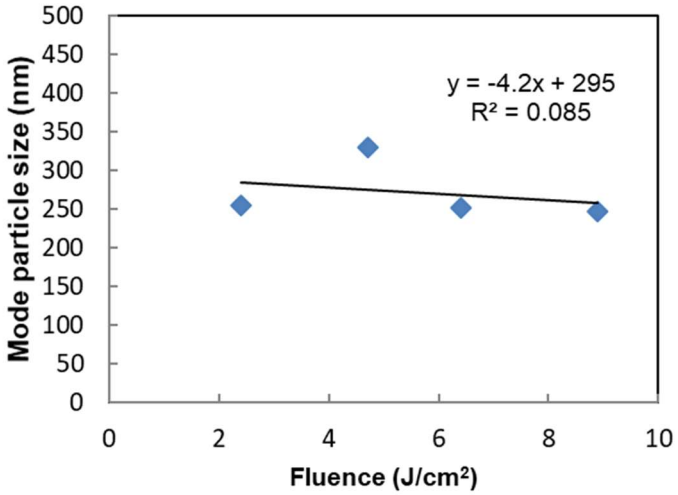

Fig. 2-8 (a) Secondary particle size distribution,
(b) mode secondary particle size at each fluence by DLS.

NPs have a property of extremely high adhesion and aggregation, but especially when the particle size is 10-100 nm, the chemical properties, physical properties, and functions change significantly compared to when the particle size is larger[2-11]. Besides, form Kamiya and Iijima's simulation results of the sum of the interfacial electric double layer, repulsive potential, and van der Waals attraction based on the DLVO theory (the potential changes depending on the surface potential, particle size, and counterion concentration), 300 nm sized particles could disperse, whereas 20 nm sized particles aggregate. 20 nm sized particles concentration increase, it also results in easy aggregate. This simulation

results support our consideration of (2) the possibility of aggregation.

Easy particle accumulation is different to the organ type, but 10-200 nm NPs correspond to a wide range of organs to accumulate. Therefore, fine NPs produced by LAL are preferable[2-12]. Furthermore, considering the mixing with Ce6, fine NPs are effective to well mixture efficiency. Therefore, to obtain fine NPs, countermeasures for (1) grain gradient and (2) aggregation are shown below.

Countermeasure for (1) is effective to do classification by centrifugation or filtering. Countermeasure for (2) is pH adjustment or surface coating to raise surface potential which results to aggregation prevention[2-11]. However, in this research, since the Gd_2O_3:Er, Yb NPs are for bio medical application, pH adjustment is not suitable (pH is needed to control ~7.4 in the body[2-13]). Regarding surface coating material, it is ideal that they have the function of increasing biocompatibility and surface potential.

2.3.1.5 Fluorescence intensity by PL

Fig. 2-9 shows photoluminescence spectroscopy obtained by the prepared UCNPs when irradiating NIR (980 nm). From Fig. 2-9, light emission peaks were obtained around 410 (blue), 560 (green), and 660 nm (red). These are within visible light. And these three emissions are specific to Er. Especially, red area emission is strongest which can be strongly absorbed by photosensitizer Chlorine e6. It is considered that red emission was enhanced by host matrix Gd_2O_3. Thus, it is considered Er was doped in Gd_2O_3 same as Yb, and the desired visible light via UCNPs from NIR was obtained successfully.

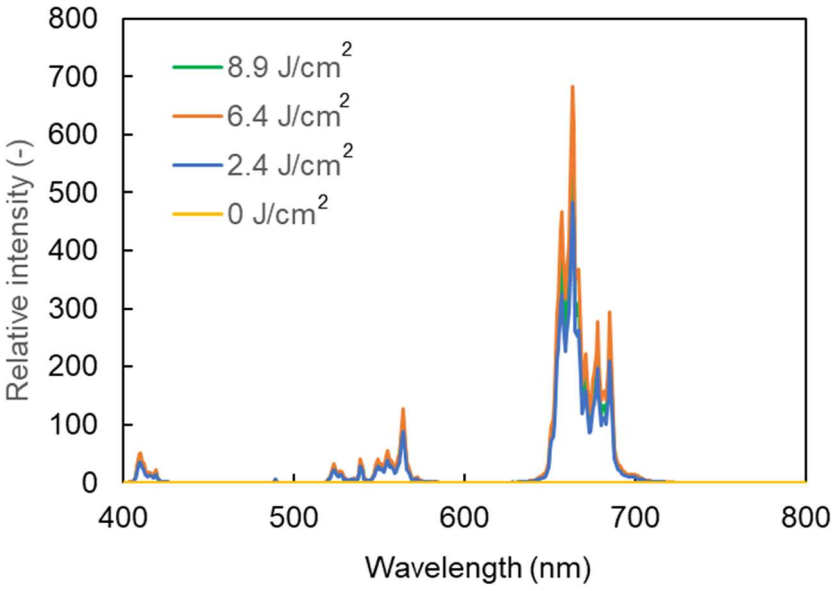

Fig. 2-9 Photoluminescence spectroscopy of prepared NPs (λ_{ex}= 980 nm, photomultiplier= 700 V, slit= 1.0 nm).

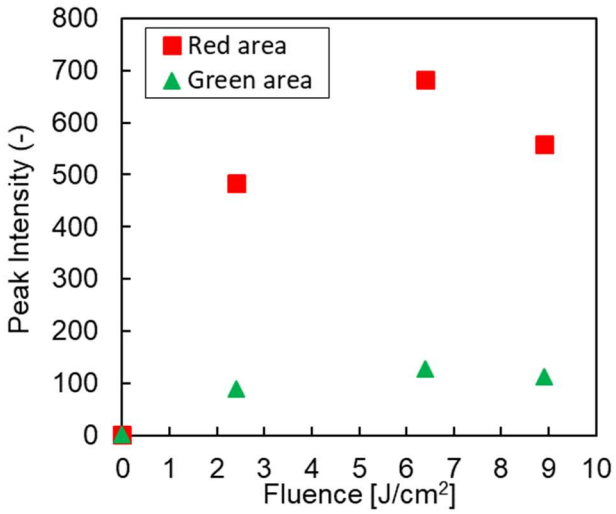

Fig. 2-10 Peak PL intensity of prepared NPs.

Fig. 2-10 shows extracted peak PL intensity in the green and red area of Fig. 2-9. The peak PL intensity increased until the middle fluence as the fluence increased. At a high fluence, the peak PL intensity slightly decreased. Increase of PL intensity until middle fluence is caused by increase of NPs number along to the fluence increase. Slightly decrease of PL intensity at high fluence is caused by fine NPs properties.

As the particle size decreases, the specific surface area (ratio of surface area per weight) increases[2-14]. This means the ratio of surface defects (kinks and steps) also increases compared to larger NPs. Surface defects leak the energy of the excited state as non-radiative deactivation which finally results in heat energy not for light emission (energy loss). This specific surface area is also affected to dangling bond on the surface. Dangling bond is sp^3 hybrid orbital with no coupling hand, also exists on the surface. They want to find binding partner to become stable energy state, but un coupling state remain their energy state unstable. sp^3 hybrid orbital behave electron donating, provide energy to others. It can be said excited energy also be leaked to dangling bond (energy loss for photoluminescence). This dangling bond existence is also relatively high when specific surface area increase.

Above all, fine NPs states results to increase of energy loss caused by relatively increased surface defects ad dangling bond along to increase of specific surface area. Therefore, peak PL intensity decreased at high fluence, compared to middle fluence which still also contains more coarse NPs.

2.3.1.6 Photon number

There is relation between emission and excitation as following[2-15],

$$P_{em} = A\, P_{ex}^{\,n} \quad (1)$$

(P_{em}: emission intensity, P_{ex}: excitation intensity, n: photon number, A: constant)

Taking the logarithm of both sides gives a linear equation as follows:

$$\log (P_{em}) = n \log (P_{ex}) + C \quad (2)$$

(C: constant)

This equation shows that photon number n of NPs can be known as the slope by measuring emission light intensity of NPs and excitation intensity of light source.

Fig. 2-11 shows the result of photon number measurement of prepared NPs at middle and high fluence. The photon number was calculated as slope from the data of varied excitation light intensity (λ_{ex}= 980 nm) and accumulated emission light intensity at red area (610-750 nm). n = 2.4 and 3.2 at the middle and high fluence, respectively. Photo number n increased toward the high fluence.

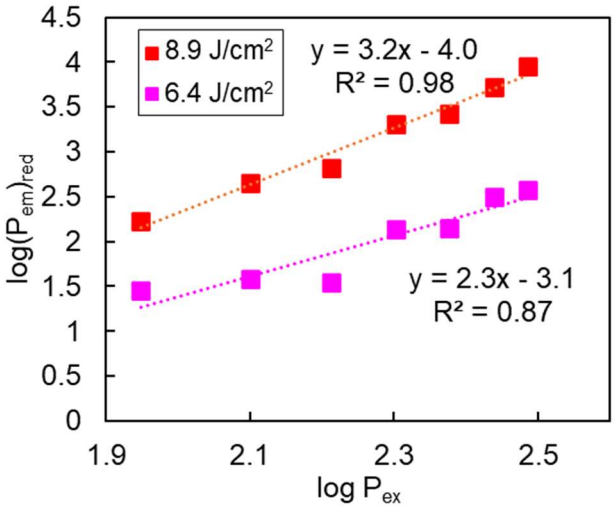

Fig. 2-11 Photon number measurement of prepared NPs at middle and high fluence (λ_{ex}= 980 nm, photomultiplier= 700 V, slit= 1.0 nm).

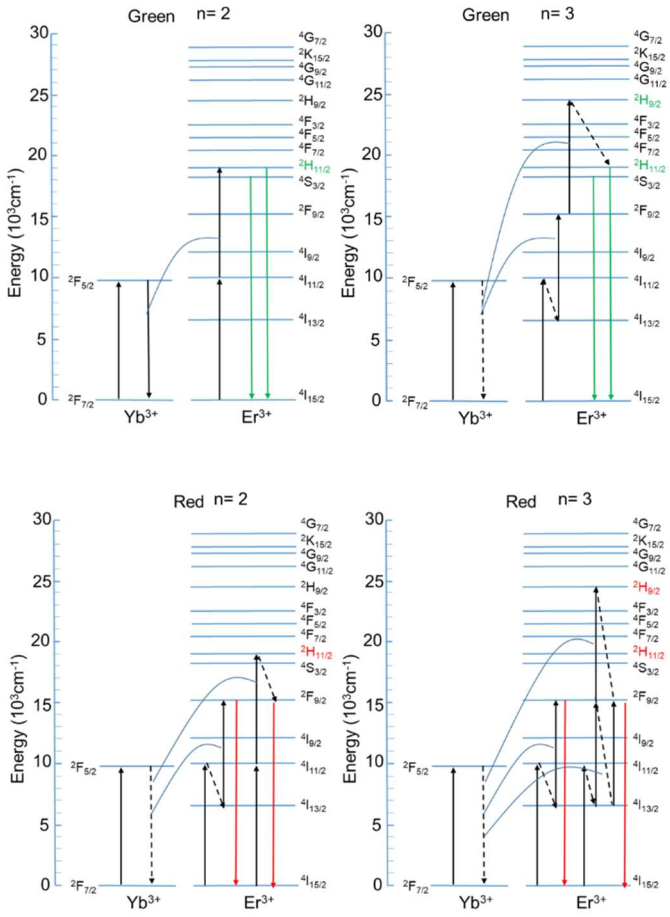

Fig. 2-12 Energy diagram of excitation and emission.

Table. 2-1 Times of energy loss of each emission process

Photon number	Emission light	Non-radiative deactivation (finally heat energy)	Cross-relaxation	UC emission efficiency
n= 2	Green	0	0	High
	Red	2	0	Middle
n= 3	Green	2	0	Middle
	Red	1	1	Low

↑

Energy transfer:
Er^{3+} →"another Er^{3+}"
Yb^{3+}→Er^{3+}

High efficiency

UC efficiency
・Most efficient: Energy transfer between excited ions
・Next most efficient: Absorption from excited state

As shown in Fig. 2-12, depending on photon number *n*, their process for luminescence are different[2-15]. Dashed allow in Fig. 2-12 means energy loss by non-radiative deactivation or cross-relaxation. The less energy loss, more effective emission process. In Table. 2-1 shows times of energy loss of each emission process according to Fig. 2-12. Especially, energy transfer by cross-relaxation from Er to Er is less efficient than energy transfer from Yb to Er[2-16].

According to these, getting back to the consideration for Fig. 2-11, photon number increase are considered to be effected by fine NPs. Fine NPs has large specific area and effect of surface defect and dangling bond became larger which result to energy loss. They make defect levels which activated energy to leak. Therefore, NPs at high fluence became photon number *n*= 3 (less emission efficiency process).

2.3.2 Effect of laser irradiation time on NPs by LAL[2-17]

2.3.2.1 Primary particle size by SEM and distribution

Fig. 2-13 shows SEM images after (a) 5 min, (b) 15 min, (c) 30 min laser irradiation (5.7 J/cm^2). From Fig. 2-13 (a), after 5 min laser irradiation, aggregated or single condition of coarse NPs (d> 200 nm) were in shape angular or spherical. There were also few fine NPs (d< 100nm) which in shape spherical. From Fig. 2-13 (b) and (c), after 15, 30 min laser irradiation, isolated coarse NPs decreased and spherical. Fine NPs increased compared to 5 min and spherical.

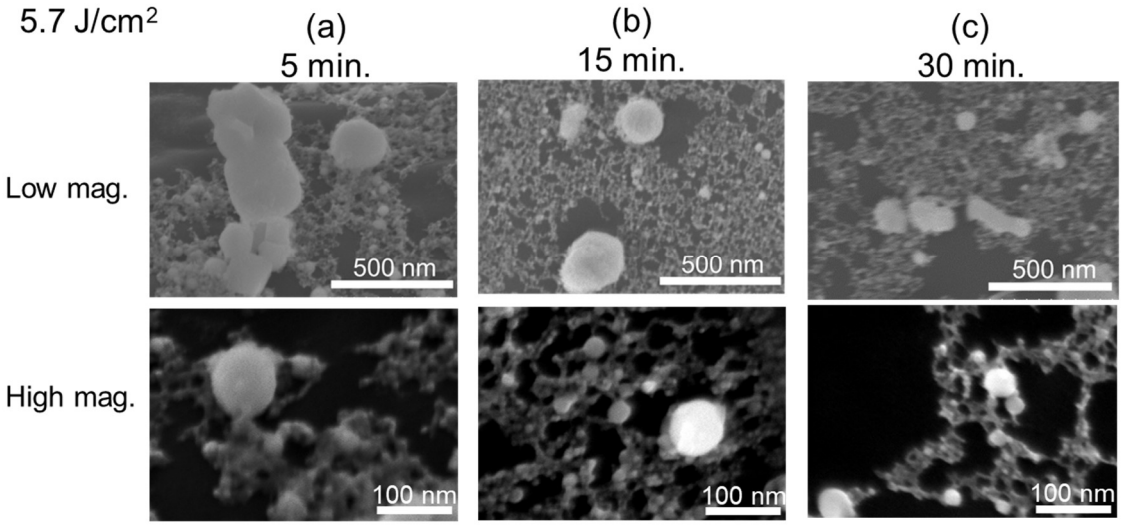

Fig. 2-13 SEM images after (a) 5 min, (b) 15 min, (c) 30 min laser irradiation (5.7 J/cm^2).

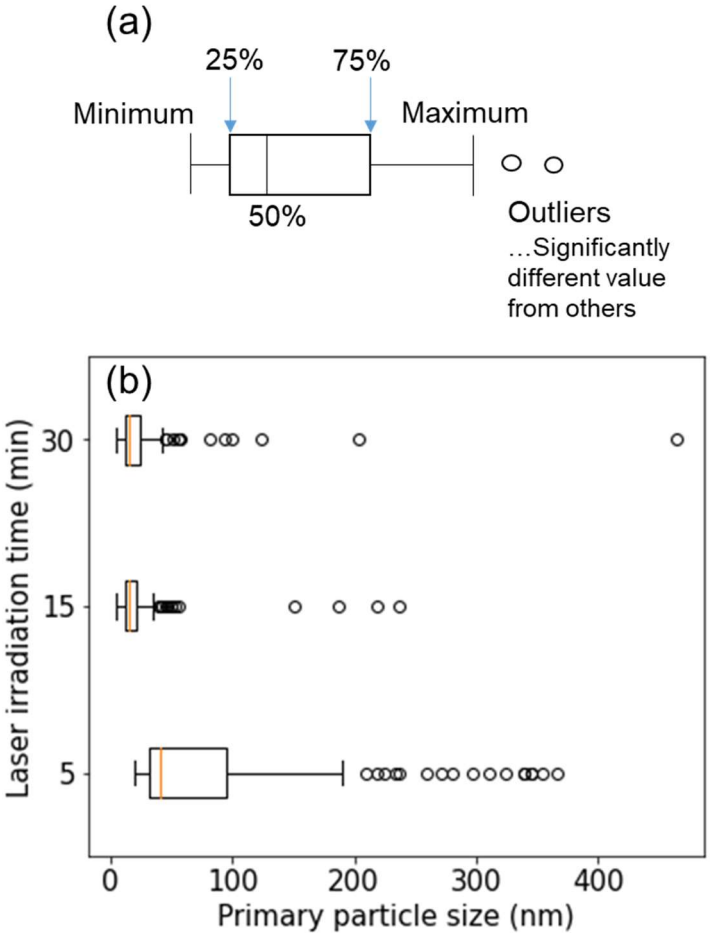

Fig. 2-14 (a) Explanation of box plot, (b) box plot of primary particle size.

Fig. 2-14 shows (a) explanation of box plot, (b) box plot of primary particle size. The box plot was obtained from the SEM primary particle size data measured by Nanomeasure and programming by Google colaboratory. The boxplot is the results assuming that the data follow a standard normal distribution.

From Fig.2-14 (a), left end of rectangle is 25%, right end of rectangle is 75 %, and vertical line in rectangle is 50 % of data when the data in order from small. Outside of rectangle, the left vertical line is minimum and the right vertical line is maximum. Circles that locate outside of maximum vertical line is outliers which is significantly different values from other estimated values.

From Fig.2-14 (b), primary particle distribution tendency can be known. Minimum and miximum value were (5 min) 19 nm, 187 nm, (15 min) 3 nm, 35 nm, (30 min) 3 nm, 41 nm. The range of outliers was (5 min) 206-362 nm, (15 min) 37-235nm, (30 min) 44-460 nm. As over all tendency, particle size range became narrow with laser irradiation time. And composition became similar from 15 min irradiation.

2.3.2.2 Secondary particle size by DLS

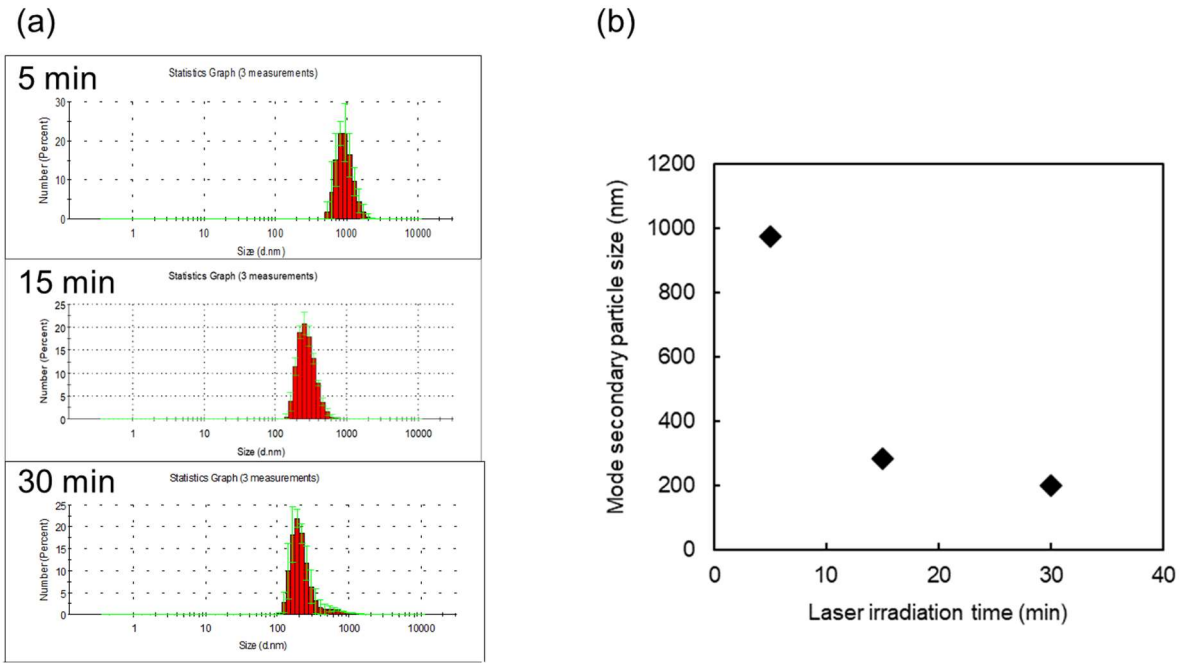

Fig. 2-15 (a) Secondary particle size distribution, (b) mode secondary particle size at each irradiation time by DLS.

Fig. 2-15 shows secondary particle size results by DLS. From Fig. 2-15 (a), obtained distribution was unimodal at each irradiation. As irradiation time increased, the peak shift to left.

In Fig. 2-15 (b), mode particle size at each irradiation time was picked up. Mode particle size was ~ 1000 nm (5 min), decreased to ~ 200 nm (15, 30 min). Secondary particle changing tendency was similar from 15 min which is same to primary particle size.

2.3.2.3 Fluorescence intensity by PL

Fig. 2-16 shows photoluminescence spectroscopy obtained by the prepared UCNPs when irradiating 980 nm near infrared light. From Fig. 2-16, light emission peaks were obtained around 410 (blue), 560 (green), and 660 nm (red). These are within visible light wavelength. The desired visible light via upconversion NPs from near-infrared light was obtained successfully at each laser irradiation time.

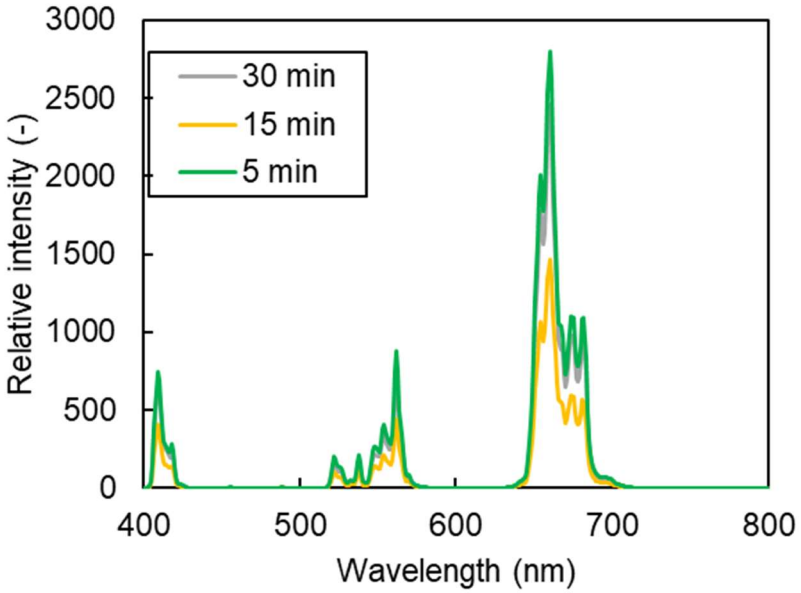

Fig. 2-16 Photoluminescence spectroscopy of prepared NPs at each laser irradiation time (λ_{ex}= 980 nm, photomultiplier= 700 V, slit= 2.5 nm).

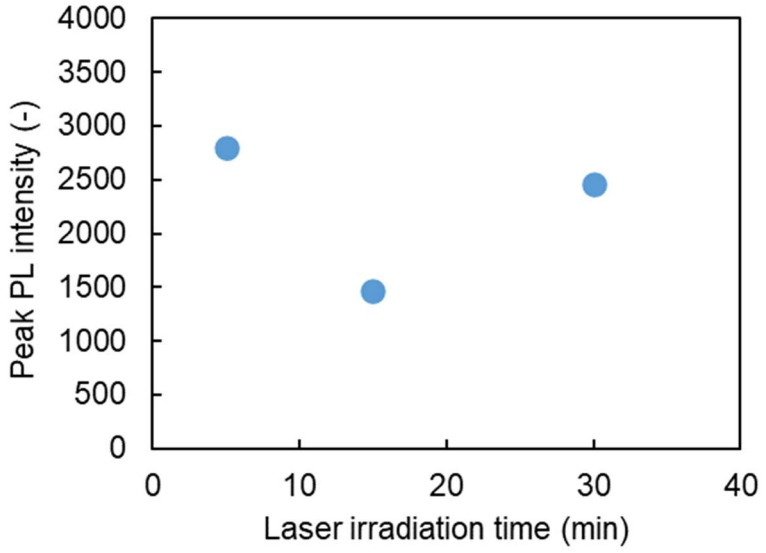

Fig. 2-17 Peak PL intensity of prepared NPs at each laser irradiation time.

Fig. 2-17 shows extracted peak PL intensity in the green and red areas of Fig. 2-16. Peak PL intensity was decreased from 5 to 15 min and increased 15 to 30 min. This changing is considered by following factors: at 5 min, strong emission was from large particles. At 15 min, PL intensity decreased because of decreased large particles and

increased smaller NPs which have small emission efficiency that larger particles. At 30 min, although smaller NPs increased, total amount of them increased, therefore, PL intensity was increased again.

2.3.2.4 Photon number

Fig. 2-18 shows photon number measurement of prepared NPs at each laser irradiation time. Slope of equation is photon number *n*. From Fig. 2-18, photon number was $n \sim 2$ at each irradiation time and have not changed.

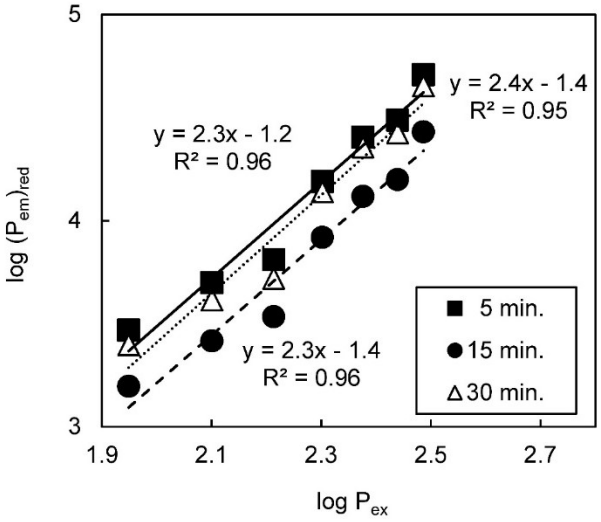

Fig. 2-18 Photon number measurement of prepared NPs at each laser irradiation time (λ_{ex}= 980 nm, photomultiplier= 700 V, slit= 2.5 nm).

2.3.2.5 Zeta potential

Fig. 2-19 shows zeta potential of prepared NPs at each laser irradiation time. Zeta potential shows stability due to their repulsion between surface charges. From Fig. 2-19, at 5 min, most stable zeta potential 25 mV. At 15 and 30 min, stability decreased around 15-20 mV. The 5 min value was from large particles and decreased zeta potential from smaller particles. However, at each laser irradiation time, zeta potential was > 15mV, relatively stable.

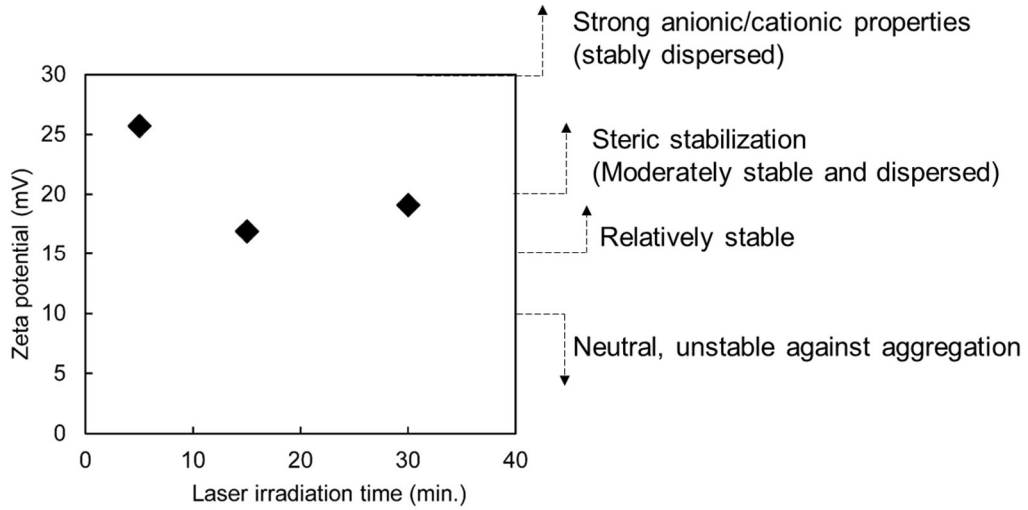

Fig. 2-19 Zeta potential of prepared NPs at each laser irradiation time.

2.3.3 Classification

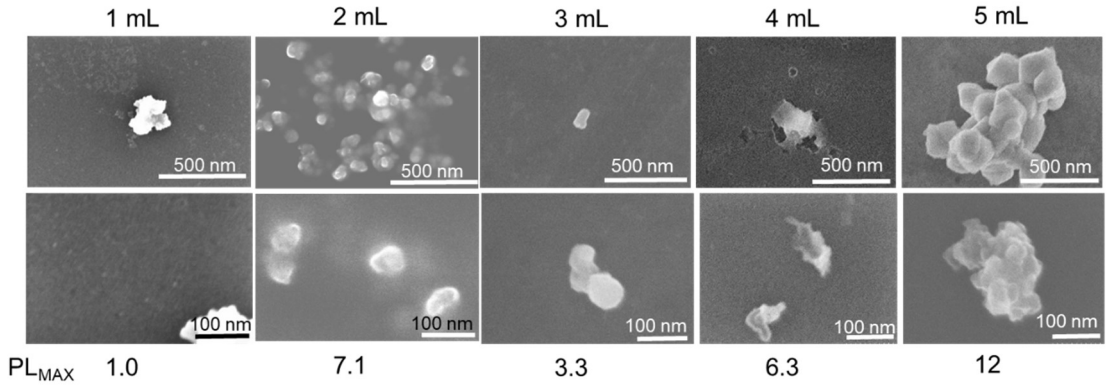

Fig. 2-20 SEM images of NPs after centrifugation and peak PL intensity (at 660 nm).

Fig. 2-20 shows SEM images of NPs after centrifugation and peak PL intensity (at 660 nm). From Fig. 2-20, in 1 mL liquid from above, almost no particles were observed. Subsequently; (2 mL) mostly sphere like d~ 80 nm fine NPs, (3 mL) few different shape of d ~ 100 nm fine NPs, larger > 400 nm particles, (4 mL) almost no fine NPs (distorted), mainly large particles (d~ μm order), and (5 mL) almost no fine NPs (distorted), mainly distorted large particles (d~ μm order) were observed. Regarding PL results, photoluminescence emission was observed from each layer.

During centrifugation, centrifugal force acts each particle in solution, as a result, particle separated in each layer in liquid according to their size and density. Larger particles exist deeper side of liquid, smaller particles exist shallower side of liquid. After

centrifugation, particles were separated as their size. Required 10-200 nm sized NPs for PDT were obtained around 2 mL from above, and they have UC emission too. From this result, required 10-200 nm and narrow distribution of NPs for PDT can be obtained after centrifugation (5000 rpm×20 min), and taking around 2 mL in liquid from above top.

2.4 Summary

2.4.1 Effect of laser intensity (fluence) on NPs by LAL

Raw material became NPs by LAL while maintaining their component element Gd, O, Er (TEM-EDS) and crystal structure (cubic and monoclinic of Gd_2O_3) with no by-products generation (XRD). Coarse NPs which primary particle size is 200-300 nm were obtained at low fluence (~2-5 J/cm^2) and middle fluence (~6 J/cm^2). Fine NPs which primary particle size within 100 nm were generated from middle fluence and they increased at high fluence (~9 J/cm^2). Corse NPs were generated by fragmentation caused by the shock of laser hitting because the primary particle size is similar to the raw material's one. On the other hand, since fine NPs diameter is smaller than raw material's one, it is generated by LAL which can be started from atomic nucleation and nuclei growth. Since LAL has a threshold, it is considered that over-middle fluence is beyond the threshold. Mode secondary particle size was changed within the range of 250-350 nm at each fluence (DLS). When irradiating NIR, UCNPs emitted visible light (410 nm (blue), 560 nm (green), and 660 nm (red)) which are specific emissions to Er. In particular, red area emission is strongest which can be strongly absorbed by photosensitizer Chlorine e6. Enhanced red emission is caused by host matrix Gd_2O_3. Thus, it is considered Er was doped in Gd_2O_3 same as Yb (PL). The photon number was n = 2.4 and 3.2 at the middle and high fluence, respectively. photon number increase are considered to be affected by fine NPs. Fine NPs have a large specific area and the effect of surface defect and dangling bond became larger which result in energy loss.

2.4.2 Effect of laser irradiation time on NPs by LAL

From the result of primary particle size observation (SEM), there were many coarse NPs and few fine NPs at 5 min, but after 15 min, the coarse NPs decreased and fine NPs increased. From the result of secondary particle size measurement (DLS), mode secondary particle size was 1000 nm at 5 min, but decreased to about 200 nm at 15 and 30 min. Photoluminescence decreased once from 5 to 15 min but increased after 30 min again (PL). This is considered to be determined by the composition of coarse NPs and fine NPs and overall amount of particles. From the result of photon number, there was no change in the number of photons at any laser irradiation time. The most stable value was

shown at 5 min, but it was >15 mV at all laser irradiation times, which was a relatively stable state (Zeta potential).

From above all results on morphology, emission properties, and stability, similar properties of NPs colloidal solution can be obtained after 15 min laser irradiation

2.4.3 Classification

NPs solution was made at fluence 9.0 J/cm^2, and laser irradiation time 15 min. All of the obtained NPs solution (6 mL) were centrifugated (5000 rpm × 20 min) for particle classification. The required 10-200 nm and narrow distribution of NPs for PDT obtained after centrifugation (5000 rpm×20 min), and taking around 2 mL in liquid from above top.

2.5 References

[2-1] K. O. Aiyyzhy, E. V. Barmina, V. V. Voronov, G. A. Shafeev, G. G. Novikov, and O.V. Uvarov, Opt. Laser Tech., 155, (2022), 108393.

[2-2] S. Hashimoto, Rev. Laser Eng., 45, (2017), 1.

[2-3] T. E. Itina, J. Phys. Chem. C, 115, (2011), 5044.

[2-4] N. Livakas, E. Skoulas, and E. Stratakis, Opt. Electron. Adv., 3, (2020) 190035.

[2-5] B. K. Pandey, A. K. Shahi, J. Shah, R. K. Kotnala, and R. Gopa, Appl. Surf. Sci., 289, (2014), 462.

[2-6] K. Sasaki, J. Plasma Fusion Res., 86, (2010), 324.

[2-7] S. Reich, P. Schönfeld, A. Letzel, S. Kohsakowski, M. Olbinado, B. Gökce, S. Barcikowski, P. Doz., and A. Plech, Chem Phys Chem, 18, (2017), 1084.

[2-8] J. A. Feshitan, C. C. ChenJames, J. K. Mark, and A. Borden, J. Colloid Interface Sci., 329, (2009), 316.

[2-9] Y. Tei, H. Wang, Y. Kitamoto, M. Hara, and H. Wada, J. Laser Micro/Nanoeng., 16, (2021), 115.

[2-10] B. Soltani, B. Azarhoushang, and A. Zahedi, Opt. Laser Tech, 119, (2019), 105644.

[2-11] H. Kamiya and M. Iijima, The Micromeritics, 55, (2012) 12.

[2-12] N. Khlebtsov and L. Dykman, Chem. Soc. Rev., 40, (2011), 1647.

[2-13] Y. Ito, Y. Yuzawa, and S. Matsuo, J. Jpn. Soc. Intern. Med., 95, (2016), 45.

[2-14] S. Takeshita, J. Jpn. Soc. Colour Mater., 88, (2015), 106.

[2-15] Y. Onodera, T. Nunokawa, O. Odawara, and H. Wada, J. Lumin., 137, (2013), 220.

[2-16] The Japan Society of Applied Physics and Optical Society of Japan: Bisho-kogaku handbook, (Asakura Publishing, 1997) pp.500-509.

[2-17] Y. Tei, Y. Kitamoto, M. Hara, and H. Wada, Appl. Phys. A, 128, (2022), 789.

Chapter 3
Surface coating on NPs

3.1 Introduction

Coating the surface of NPs for biomedical applications (used in the body) with a high biocompatibility material can prevent extraction from the body which is caused by the immune system regarding them as foreign substances. Furthermore, in the case of the UCNPs, enhanced fluorescence emission can be increased because surface defects are coated. In addition, it has the effect of preventing agglomeration and improving solubility and dispersibility[3-1].

Surface coating materials with high biocompatibility include polyethylene glycol (PEG), polyvinylpyrrolidone (PVP), and SiO_2, etc.

Coating the surface of NPs with PEG improves their retention in the blood and makes them more difficult to eliminate from the outside[3-2], increasing the efficiency of NPs transport to the target site. For PEG coatings, the thicker the film, the better the retention. The film thickness increases as the PEG molecular weight increases, but the coating rate decreases (a trade-off relationship). From these, PEG with a molecular weight of 2000-5000 are often selected, and PEG2000 is said to be the most suitable. The larger the molecular weight of PEG, the more it takes on a mushroom structure[3-3].

Coating the surface of NPs with PVP adds properties such that they are not regarded as foreign substances by the immune system (immunogenicity) and rarely bind to substances in the body (antigenicity)[3-4]. Additionally, since it is amphiphilic, it can be adsorbed onto various materials (Au, Ag, iron oxide, alumina, silica, etc.)[3-5].

Silica is a biocompatible material used in bone repair and DDS[3-6], has chemical stability, and can make the surface of hydrophobic NPs hydrophilic[3-7]. Besides, it is a reasonable cost and has high optical transparency and photochemical stability even under laser photolysis[3-1].

In this chapter, PEG coating on NPs during the LAL was performed, and the enhancement of luminescence intensity was investigated. Adding to it, it is investigated whether PVP coating and PVP-SiO_2 coating on the Gd_2O_3 surface is possible or not, and the difference between them in luminescence intensity.

3.2 Experimental

3.2.1 PEG coated NPs by LAL

To enhance light emission efficiency and improve dispersibility and biocompatibility, surface coating was conducted.

The same laser equipment in Fig. 2-3 was used for making PEG-coated NPs. Laser intensity (fluence) was set at one strength (8.9 J/cm^2), and laser irradiation time was 30 min. The pellet was soaked in PEG solution of 0, 0.1, 1 mM concentration. Approximately

50 μL supernatant of the obtained solution was dried on Cu grid (Okenshoji Co., Ltd., elastic carbon membrane, ELS-C10), and their morphology was observed by SEM (same as 2.2.3.2 (3)). 1 mL supernatant of the obtained solution was measured by their UC emission by PL (light source: 980 nm laser diode, same as 2.2.3.2 (5)).

3.2.2 Fabrication of polyvinyl pyrrolidone (PVP) and PVP-SiO_2 coated NPs

To ensure the total amount of starting material, the powder after "Firing (2.2.1 Step 3)" process was used. By modified stöber method, PVP was coated on NPs first. Subsequently, SiO_2 was coated after PVP coating process.

(1) PVP coating

The 0.1g Gd_2O_3:Er,Yb powder after firing process and 0.40 g PVP (K30, Mw= 40,000, 3.66×10^{-2} mol/mol (PVP/Gd_2O_3)) were mixed in 100 mL pure water under stirring for 24 hours (350 rpm). The solution was poured into a plastic tube and centrifugated (5000 rpm, 30 min) to separate Gd_2O_3:Er,Yb-PVP and liquid. Obtained Gd_2O_3:Er, Yb-PVP was washed by 90 vol% acetone and centrifugated (5000 rpm, 10 min) for washing. This acetone-washing process was repeated 3 times. Washed powder was dried by vacuum drying (AS ONE, AVD-250V) overnight at 60℃. Dried powder was approximately 0.075 g. Obtained Gd_2O_3:Er, Yb-PVP powder was dispersed in 75 mL ethanol and ultrasonicated for 15 min.

A solution including Gd_2O_3:Er,Yb-PVP were dried on Cu grid (Okenshoji Co., Ltd., elastic carbon membrane, ELS-C10) and observed their morphology by SEM (same as 2.2.3.2 (3)). The composition was analyzed by TEM-EDS (same equipment as 2.2.3.2 (1)). Also, 1 mL solution including Gd_2O_3:Er, Yb-PVP was measured by PL (same as 2.2.3.2 (5)).

(2) SiO_2 coating

0.75 g PVP- Gd_2O_3:Er, Yb powder, 0.063 g tetra ethoxy silane (TEOS, 1.47 mol/mol (TEOS/ Gd_2O_3)), and 6.19 mL 30% NH_4OH were mixed under stirring for 2 hours (300 rpm). The solution was poured into a plastic tube and centrifugated (5000 rpm, 30 min) to separate Gd_2O_3:Er,Yb-PVP-SiO_2 and liquid. Obtained Gd_2O_3:Er,Yb-PVP-SiO_2 was washed by 50 vol% acetone and centrifugated (5000 rpm, 10 min) for washing. This acetone-washing process was repeated 3 times. Washed powder was dried by vacuum drying overnight at 60℃. Dried powder was approximately 0.06 g.

Obtained Gd_2O_3:Er,Yb-PVP-SiO_2 was observed by TEM-EDS and SEM (same equipment as 2.2.3.2 (1) and (3)). 1 mL solution Gd_2O_3:Er,Yb-PVP-SiO_2 in water was

measured by PL (same as 2.2.3.2 (5)).

3.3 Results and discussion

3.3.1 Fabrication of polyethylene glycol (PEG) coated NPs by LAL

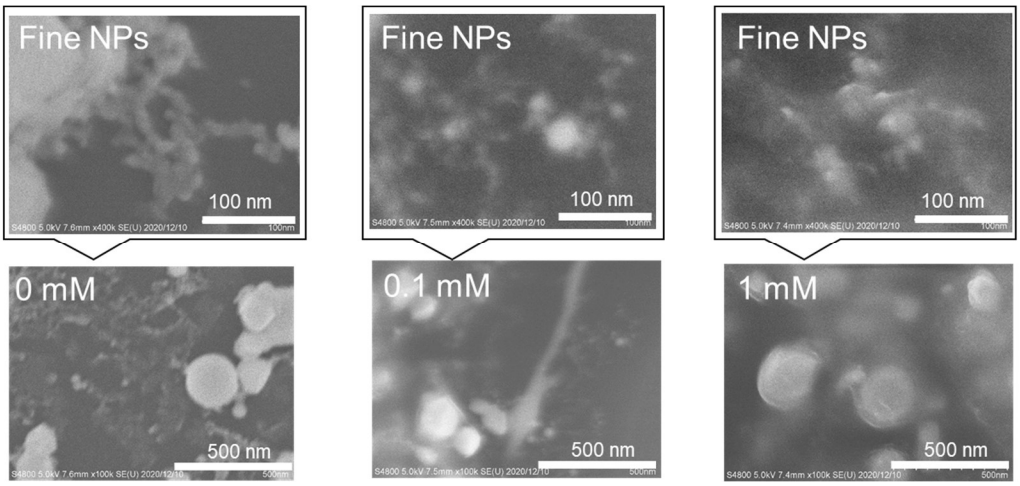

Fig. 3-1 SEM images of NPs generated in PEG solution by LAL.

Fig. 3-1 shows SEM image of NPs generated in PEG solution by LAL. From the SEM result of 0 mM PEG solution (water), coarse NPs (d > 200 nm) and fine NPs (d < 100 nm) are observed. From the SEM result of 0.1 mM PEG solution, the observed shape became vague compared to 0 mM case, it is considered PEG was coated around NPs. Overall coarse NPs were decreased and d< 200 nm NPs were increased. From the SEM result of 1 mM PEG solution, the observed shape became vaguer compared to 0.1 mM case, it is considered because of higher PEG existence. Coarse NPs were decreased compared to 0.1 mM case.

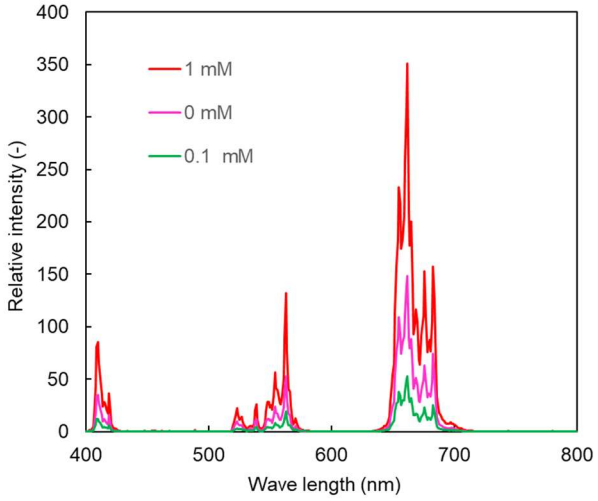

Fig. 3-2 Photoluminescence emission of obtained NPs in PEG solution.

Fig. 3-2 shows photoluminescence emission of obtained NPs in PEG solution. Emission peaks were observed in the blue area (~410 nm), green (~550 nm), and red (~660 nm) when irradiating 980 nm laser. From this result, aimed visible light via UCNPs when irradiating 980 nm was successfully obtained. As shown in Fig. 1-5, UCNPs absorbs NIR (980 nm), Yb^{3+} is electronically excited, energy is transferred to Er^{3+}, and the excited Er^{3+} returns to the ground state, emitting light (410 nm (blue, $^2H_{9/2}$), 540 nm (green, $^2H_{11/2}$), 565 nm (green, $^4S_{3/2}$) and 660 nm (red, $^4F_{9/2}$))[3-8] are obtained. The peak intensity of wavelength in Fig. 3-2 and the theoretical emission area were the same, thus, aimed UC phenomenon occurred in Gd_2O_3:Er, Yb even it is coated by PEG.

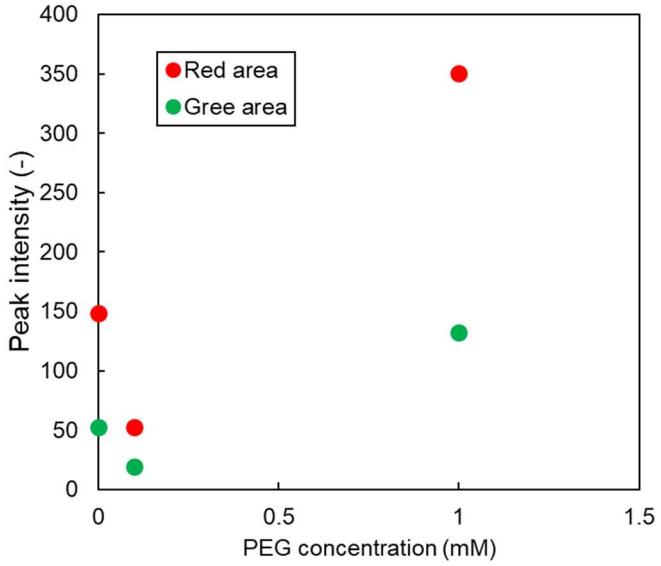

Fig. 3-3 Peak PL intensity of obtained NPs in PEG solution.

Fig. 3-3 shows peak PL intensity of obtained NPs in PEG solution from the data of Fig. 3-2. Peak intensity was once decreased at 0.1 mM, and increased at 1 mM. Decrease at 0.1 mM occurred due to decreased coarse NPs which is stronger emission than fine NPs. Increase of peak PL intensity at 1 mM occurred by surface coating effect. Surface coating is effective to coat surface defects and dangling bond which is still anxious energy state, results to energy loss at excited level. From this result, it is considered PEG coating is effective to increase emission intensity of fine NPs.

3.3.2 Fabrication of polyvinyl pyrrolidone (PVP) and PVP-SiO_2 coated NPs

(1) PVP coating

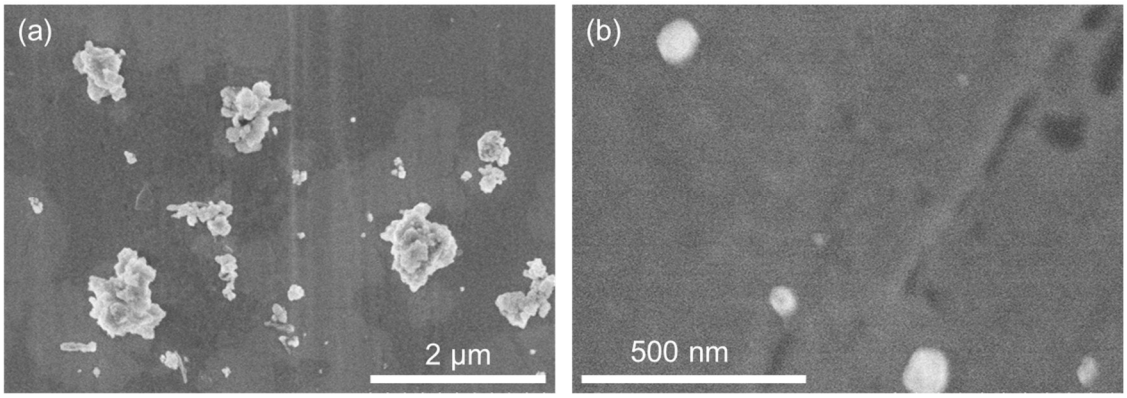

Fig. 3-4 SEM images of PVP-coated NPs at (a) low and (b) high magnification.

Fig. 3-4 shows SEM images of NPs-PVP and aggregated the μm ordered particles and isolated d~100 nm fine NPs were both observed.

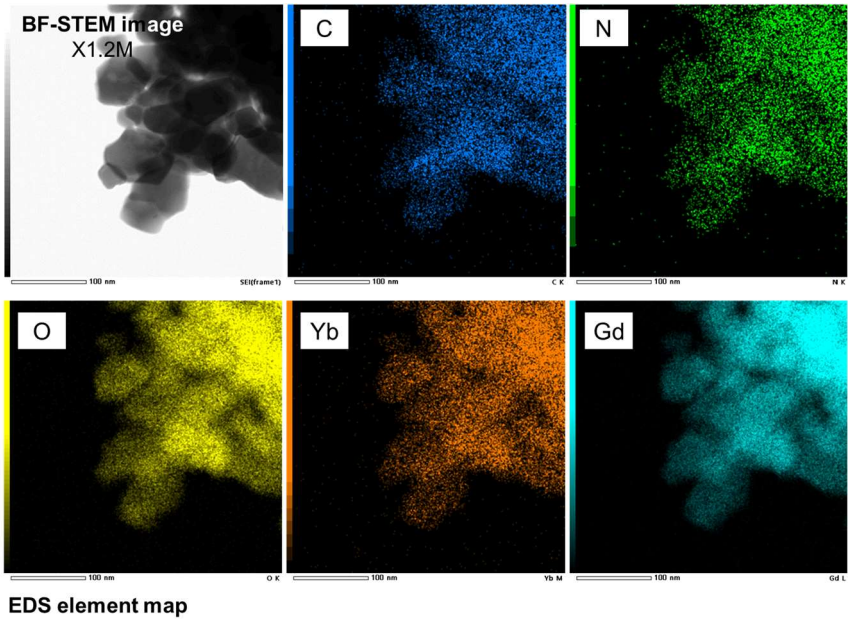

Fig. 3-5 Element analysis of PVP coated NPs by TEM-EDS.

Fig. 3-5 shows TEM-EDS element analysis results of PVP coated NPs, and particles were composed of elements of C, N, O, Yb, and Gd.

From Fig. 3-5, Gd and Yb were from original NPs. Er was not observed this time, it is because too low concentration (1 mol%) in NPs to observe. Since PVP was composed of

C, N, and O. Element of O was both from NPs and PVP. However, C and N only form PVP were on the same site on NPs, therefore PVP was successfully coated around NPs. Aggregation may have occurred during drying on the grid or by crosslinking or depletion aggregation of PVP.

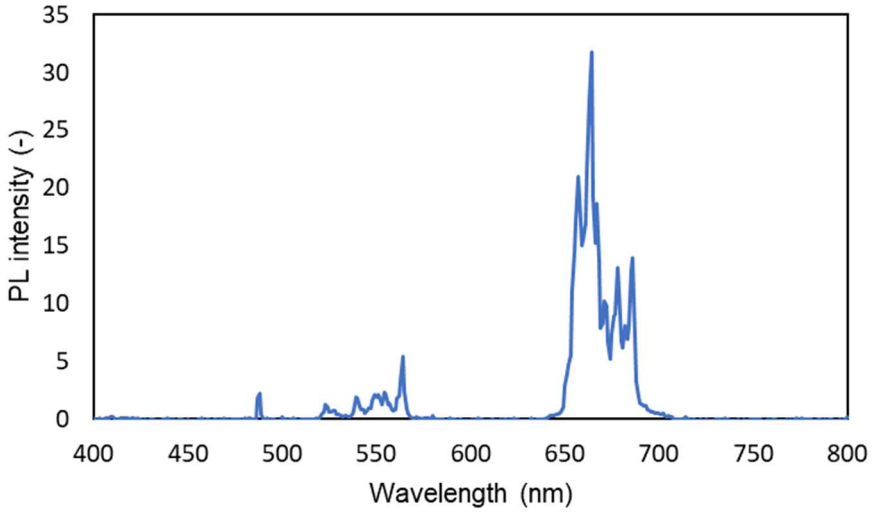

Fig. 3-6 Photoluminescence emission of PVP coated NPs.

From Fig. 3-6, visible light was obtained via PVP coated NPs from 980 nm. PVP did not change the emission wavelength of visible light and did not inhibit luminescence.

(2) SiO_2 coating

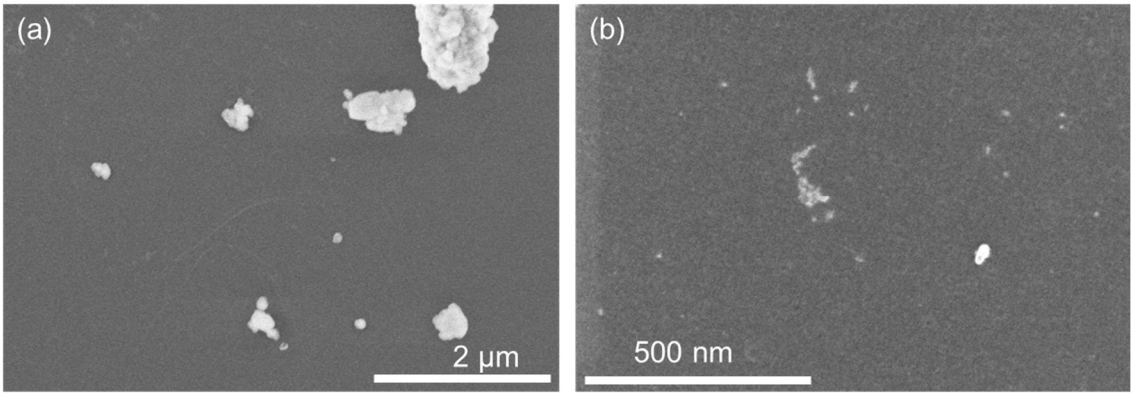

Fig. 3-7 SEM images of PVP-SiO_2 coated NPs at (a) high and (b) magnification.

From the SEM result in Fig. 3-7, there were μm-sized PVP-SiO_2 coated particles, which were even larger than PVP coated one. This was a three-dimensional agglomeration

of small particles. A small number of NPs with a diameter of ~100 nm also exists.

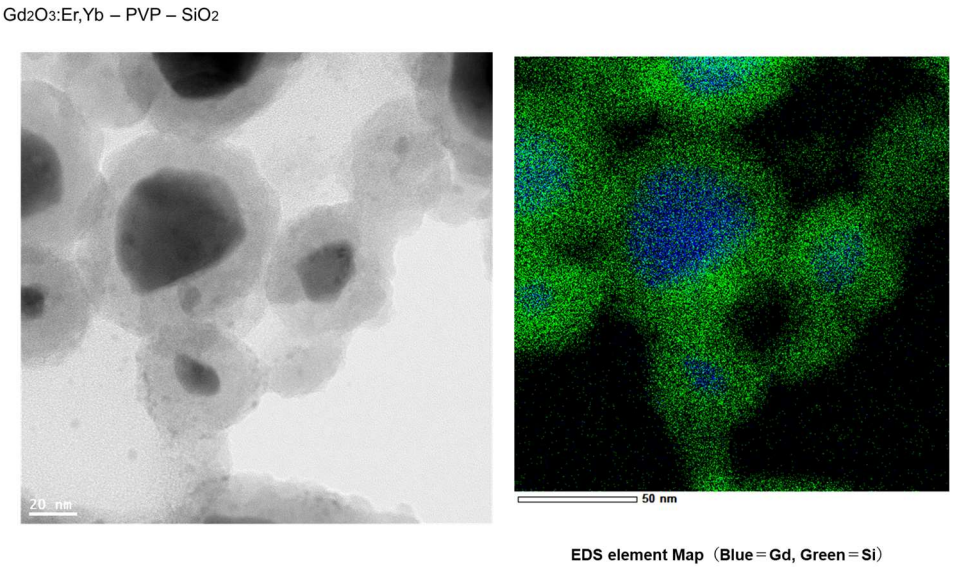

Fig. 3-8 Element analysis of PVP-SiO_2 coated NPs by TEM-EDS.

Fig. 3-8 shows TEM-EDS element analysis results of PVP-SiO_2 coated NPs, a Si layer was confirmed around the NPs containing Gd. The thickness of SiO_2 was approximately ~15 nm. From Fig. 3-8, it can be said that hydrolyze TEOS and coat SiO_2 around the PVP-coated NPs were proceeded.

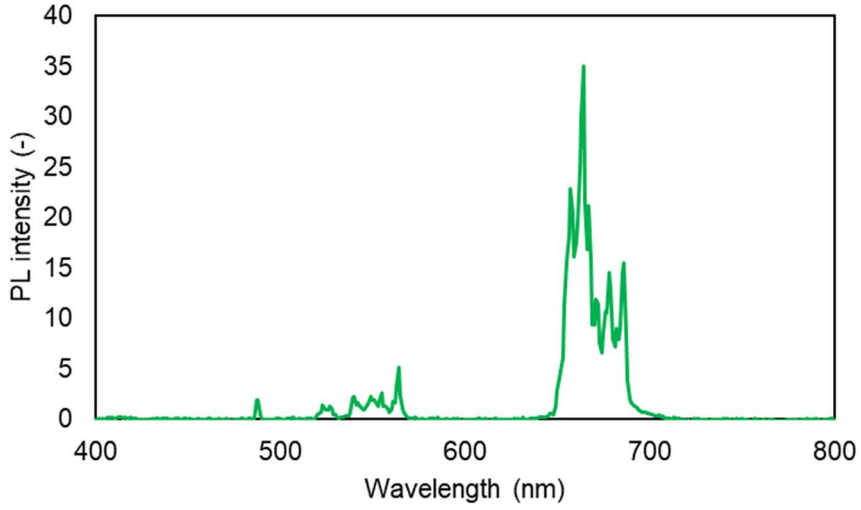

Fig. 3-9 Photoluminescence emission of PVP-SiO_2 coated NPs.

From Fig. 3-9, visible light was obtained via PVP-SiO_2 coated NPs from 980 nm.

Coating with PVP-SiO_2 did not change the visible light emission area. Furthermore, the luminescence intensities of PVP coated NPs and PVP-SiO_2 coated NPs were almost the same. From this, it is considered that once the particle surface is coated, the emission intensity will not be enhanced even if other coatings are applied to the outermost shell.

3.4 Summary

PEG coating on NPs during the LAL was performed, and the enhancement of luminescence intensity was investigated. It is investigated whether PVP coating and PVP-SiO_2 coating on the Gd_2O_3:Er,Yb surface is possible or not, and difference between them of luminescence intensity.

PEG coated NPs showed increased PL intensity which is considered due to surface defect or dangling bond (factor of energy loss) coated.

PVP and PVP-SiO_2 coating on Gd_2O_3:Er,Yb were succussed respectively. Some were 3 dimensionally aggregated due to drying on the grid or by crosslinking or depletion aggregation of PVP-SiO_2. Since PL intensity was not changed between PVP coated and PVP-SiO_2 coated, it is considered that once the particle surface is coated, the emission intensity will not be enhanced even if other coatings are applied to the outermost shell.

3.5 References

[3-1] A. Ansari, A.K. Parchur, M. Alam, and A. Azzeer, Mater. Chem. Phys., 147, (2014), 715.

[3-2] G. Zhang, Z. Yang, W. Lu, R. Zhang, Q. Huang, M. Tian, L. Li, D. Liang, and C. Li, Bio. Mater., 30, (2009), 1928.

[3-3] I. Sugiyama and Yasuyuki Sadzuka, Drug Delivery Syst., 31, (2016), 275.

[3-4] Y. Jiao, Z. Liu, S. Ding, L. Li, and C. Zhou, J. Appl. Polym. Sci., (2006), 10, 1515.

[3-5] K. Fujii, Y. Kitamoto, M. Hara, O. Odawara, and H. Wada, J. Lumin., 156, (2014), 8.

[3-6] M. Catauro, F. Bollino, F. Papale, M. Gallicchio, and S. Pacifico, Mater. Sci. Eng.: C, 48, (2018), 548.

[3-7] M. A. Malvindi, V. D. Matteis, A. Galeone, V. Brunetti, G. C. Anyfantis, A. Athanassiou, R. Cingolani, and P. P. Pompa, PLOS ONE, 9, (2014), e85835.

[3-8] F. Auzel, Chem. Rev., 104, (2004) 139.

Chapter 4
Reactive oxygen species occurrence test at cuvette scale

4.1 Introduction

Fig. 4-1 shows the summary of aimed PDT with UCNPs reaction scheme and ROS detection. Until Chapter 3, NPs preparation condition, mechanism, photoluminescence properties, particle distribution control, coating availability and optical properties were investigated. In Chapter 4, using the optimal NPs preparation condition (9.0 J/cm^2, > 15 min by LAL, second layer of solution after centrifugation), the experiments move to the next step; Obtaining visible light UCNPs from NIR, activating Ce6, and ROS. ROS is essential to destroy cancer. In Chapter 4, this ROS generation test was conducted on cuvette scale.

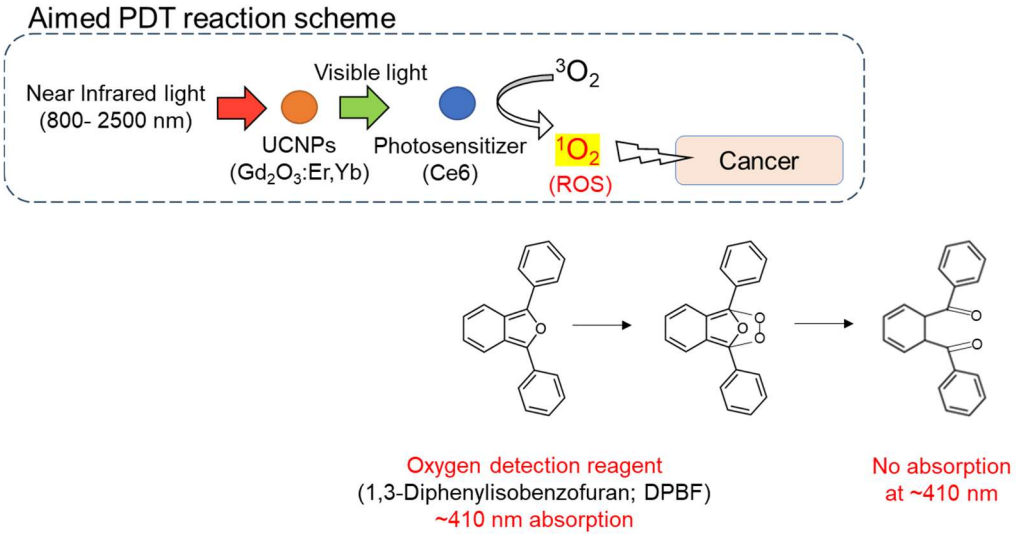

Fig. 4-1 Detection of ROS generation in PDT with UCNPs reaction scheme at cuvette scale.

To detect ROS, oxygen detection reagent: 1,3-diphenylisobenzofuran (DPBF)[4-1]is effective. DPBF has originally ~410 nm absorption but it is decomposed when exposed to ROS and became different substances which has no absorption at ~410 nm. Therefore, measuring UV-absorption when start and end time, from the absorption peak height change, ROS generation can be known.

In this chapter, it was investigated whether aimed PDT reaction using Gd_2O_3:Er,Yb UCNPs occur by confirming ROS generation.

4.2 Experimental

According to the results of NPs preparation method and classification in Chapter 2, raw material pellet and NPs solution by LAL was prepared. The obtained NPs solution was

centrifuged for narrow particle distribution which suited PDT application size. After that, ROS occurrence test at cuvette scale was conducted.

(1) Preparation of raw material (pellet)

Same as section 2.2.1.

(2) Preparation of NPs

Referring section 2.2.2, the NPs solution by LAL was prepared under following condition; laser: Nd:YAG laser, Wavelength: 532 nm, frequency: 10 Hz, pulse width: 5-7 ns, fluence: 9.0 J/cm^2, Irradiation time: 15 min.

(3) Classification

Same as section 2.2.5.1; Obtained NPs solution 6 mL was centrifugated (5000 rpm × 20 min). After centrifugation, 1mL of second layer from top and 0.6 mL of third layer from top which composed by fine NPs were used for next 4.2.(4).

(4) Reactive Oxygen Species (ROS) occurrence test in cuvette scale

Used material were below; Ce6 (98%, Combi-Blocks), DPBF (> 95.0%, Tokyo Chemical Industry Co., Ltd. (TCI))

*The following processes were performed in the dark to prevent photosensitizers from reacting with visible light.

(4-1) Preparation of solution (photosensitizer and detection regard)

100 μM DPBF solution and 170μM Ce6 solution were dissolved in ethanol and ultrasonicated 10 min for complete dissolution.

(4-2) Mixture of NPs and photosensitizer

NPs solution 2.6 mL, 100 μM DPBF 0.2 mL, 170μM Ce6 0.2 mL were poured into quartz cell. Mixture was completely mixed for 13 min until UV-absorption saturation (steady state). Stirring condition; no light, 200 rpm by stirrer (AS ONE, RS-1DN) and stirring bar (Φ3 mm×8 mm, SCS38, ASONE).

Saturated UV absorption set as starting value.

(4-3) NIR irradiation (ROS occurrence test)

Fig. 4-2 shows schematics of NIR equipment for ROS occurrence test. The light source was composed by 980 nm laser diode with temperature/current controller (ASAHI, ALP-

7433CA).

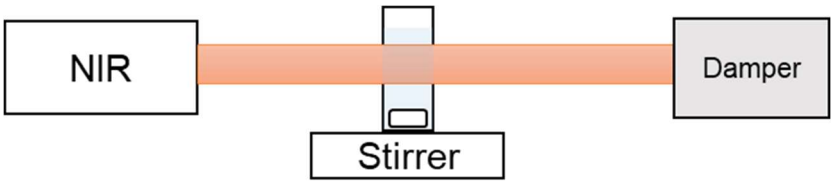

Fig. 4-2 NIR equipment for ROS occurrence test.

Using Fig. 4-2 NIR equipment, NIR was irradiated to prepared mixture. Laser irradiation condition was following; laser diameter was 0.7 cm, irradiated NIR intensity laser intensity was 0, 6.1 W/cm^2 (0, 3000 mA), irradiation time was 0,10, 20, 30 min for each NIR laser intensity, stirred at 200 rpm (CHPS-170DF, ASONE).

(5) Characterization

Absorption of DPBF was measured by Ultraviolet-visible spectroscopy (UV-vis). Measuring timing was starting state (after stirring 13 min), after 10,20, and 30 min NIR irradiation. Measuring range was 300-800 nm. The base line sample holder was water of quartz cell.

4.3 Results and discussion

4.3.1 UV-absorption raw data

Fig. 4-3 shows UV-vis absorption at (a) 0 W/cm^2 and (b) 6.1 W/cm^2. Peak 1 (~ 400 nm) was from DPBF and Ce6, and peak 2 (~ 670 nm) was from Ce6.

From Fig.4-3 (a), peak 1 was decreased from 0 min to 10 min but no value change during 10-30 min of 0 W/cm^2 NIR irradiation. On the other hand, Fig.3-4 (a) peak 2 was not decreased along 0 W/cm^2 NIR irradiation time. Therefore, decrease of peak 1 was considered to be caused by DPBF natural decomposition or other factors. Since Fig. 4-3 (a) was 0 W/cm^2 laser irradiation, DPBF is not decomposed ideally because expectation of No ROS in solution. As consideration of DPBF decrease, although experimental was performed under no light, cuvette was covered by aluminum sheet to prevent visible light it may be small amount visible light were exposed. Or more high possibility to be considered, although the solution were tried to be in steady state for first time, the mixer for steady state and the mixer using NIR equipment was different, and the stirring condition was not completely the same, therefore absorption may changed at only first 0-10 min.

From Fig. 4-3 (b), peak 1 (~ 400 nm) was decreased at each 6.1 W/cm^2 NIR laser irradiation time, peak 2 (~ 670 nm) was decreased at first 0-10 min, and after that mostly not changed. Considering the fact of no peak 2 decrease at 10-30 min, Ce6 was not decomposed by 6.1 W/cm^2 NIR. Therefore, overall decrease of 0-10 min was considered by due to the stirring condition change as same consideration of Fig. 4-3 (a). Therefore, in Fig. 4-3 (b), it can be said peak 1 (~ 400 nm) decrease at 10-30 min was from DPBF decomposition at least.

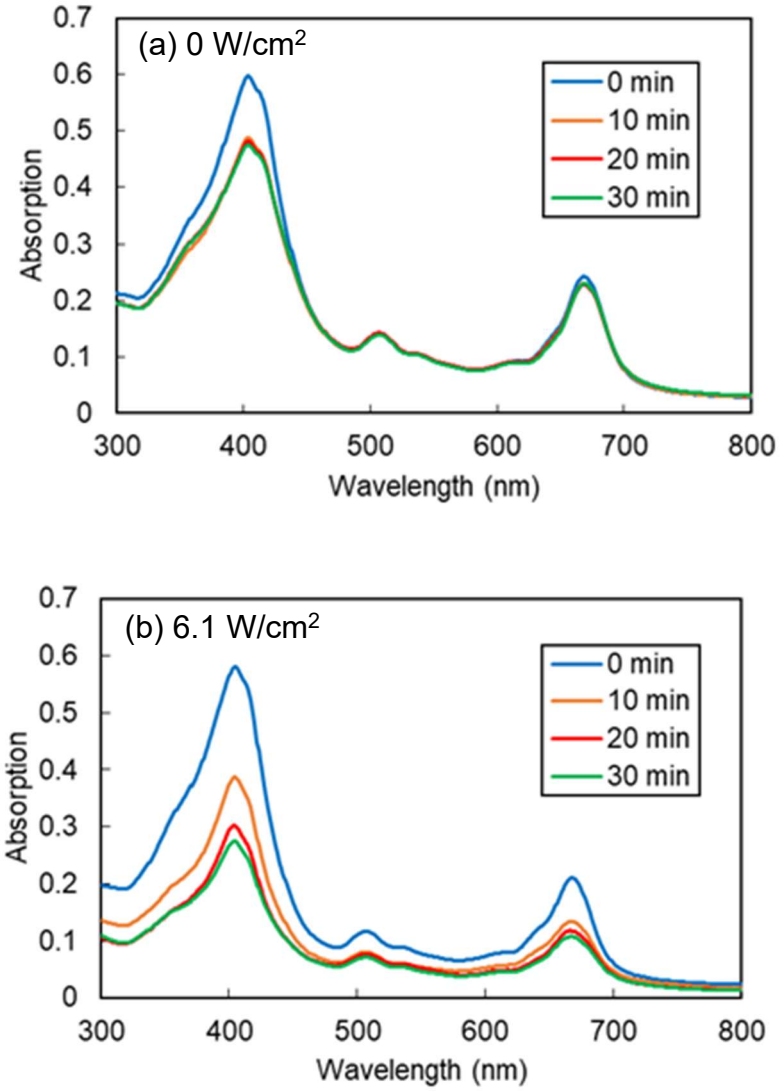

Fig. 4-3 UV-vis absorption at (a) 0 W/cm^2 and (b) 6.1 W/cm^2.

4.3.2 DPBF decrease rate

From Fig. 4-3, the peak absorption height at 404 nm (0, 6.1 W/cm^2) as DPBF decrease was picked up in Fig. 4-4. From Fig. 4-4, as NIR irradiation time increase, absorption

height was decreased. Decrease rate (slope) was - 3.2 $\times 10^{-3}$ at 0 W/cm^2 and - 7.1 $\times 10^{-3}$ at 6.1 W/cm^2. The decrease rate was large when NIR laser irradiated to solution, and its value was more than 2 times higher than no NIR laser irradiation. This is considered a significant difference. From this result, DPBF decreased due to its decomposition by reaction with ROS. Thus, aimed PDT reaction scheme with UCNPs shown in Fig. 4-1 was successfully proceeded at the cuvette scale. Also, it is realized Gd_2O_3:Er,Yb NPs can be used as this aimed PDT scheme.

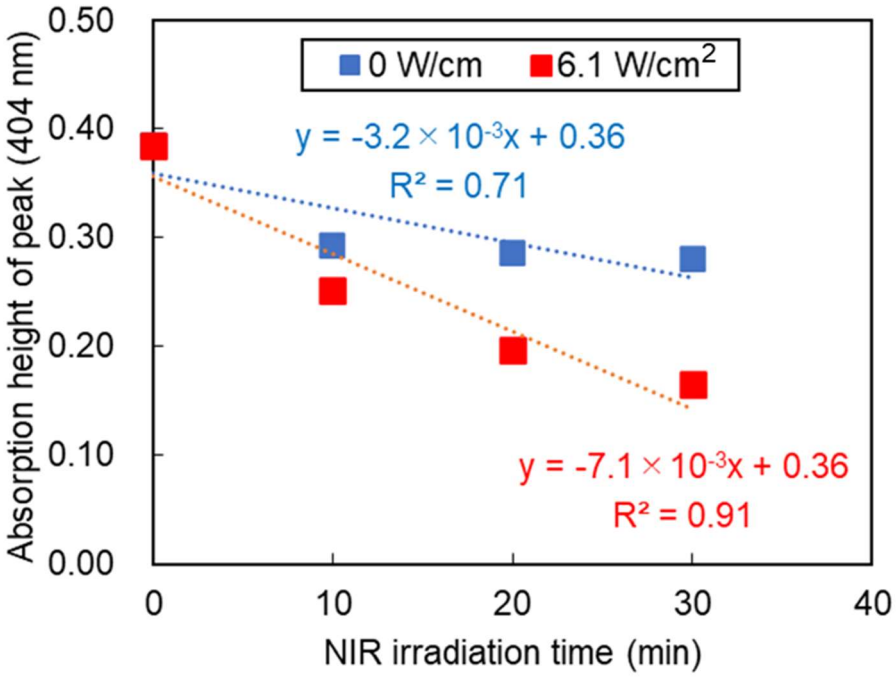

Fig. 4-4 Absorption height of peak at 404 nm (0, 6.1 W/cm^2).

4.3.3 Consideration for clinical application of PDT with UCNPs

In this study, Ce6 was activated by visible light via Gd_2O_3:Er,Yb, and ROS was generated, therefore the proposed PDT with UCNPs reaction scheme was confirmed as valid.

In clinical applications, the maximum power density of NIR is 1.0 W/cm^2. At this intensity, no obvious damage to the skin tissue is observed[4-2]. In this study, in addition to success of ROS generation at 6.1 W/cm^2, ROS generation was suggested at 3.8 W/cm^2. From these results, it is considered that reducing NIR intensity is possible by optimizing the reaction conditions. As for reaction conditions optimization, (1) UCNPs concentration, and (2) UCNPs surface coating for luminescence enhancement

per each NPs are effective. Specifically, (1) in this study, centrifugation was performed for narrow particle distribution, so the amount of particles decreased. Adding to it, the laser irradiation time was 15 min for the experiments, the total amount of produced NPs was small. Increasing laser irradiaton time to 30 min is considered to be effective to obtain larger amount of fine NPs than 15 min. Or multiple times LAL is also effective for increasing fine NPs. (2) Based on the experiments in Chapter 3, surface coating on NPs can be effective. By performing these steps (1) and (2), it is thought that the proposed PDT with UCNPs reaction can be carried out even with low NIR intensity.

4.4 Summary

ROS was successfully observed in PDT with UCNPs reaction scheme at cuvette scale.

UCNPs preparation condition was LAL (9.0 J/cm^2×15 min) and centrifugation (5000 rpm×20 min). Photosensitizer was Ce6, and oxygen detection reagent was DPBF. NIR irradiation condition was 6.1 W/cm^2 ×30 min. UV absorption was measured every 10 min.

4.5 References

[4-1] X. Zhang and X. Li, J. Lumin., 131, (2011), 2263.

[4-2] S. Lyu, Y. He, X. Tao, Y. Yao, X. Huang, Y. Ma, Z. Peng, Y. Ding, and Y. Wang, Nat. Commun., 13, (2022), 6596.

Chapter 5
Interaction between NPs and bacteria/cancer cells

5.1 Introduction

In previous chapters, NPs preparation methods and optical properties, surface coating for PDT applications, and ROS generation in solution were investigated. Since the PDT with UCNPs reaction takes place within cells, it is essential to carry out experiments to confirm whether NPs are uptaken into cells. In biological experiments, after briefly confirming interactions and safety (toxicity, adhesion, etc.) using bacteria, interaction experiments with cancer cells is conducted.

In this chapter, NIR introduced fluorescence microscope is set up originally and used to observe the behavior of NPs and biological experiments. Therefore, the objectives of this chapter is the following.

Purpose (1) Designing and building up the fluorescence microscope: 980 nm (NIR) light source was introduced to the microscope to lead fluorescence emission by UC light of individual NPs

Purpose (2) Obtain the position movie data: For the comprehension of NPs behavior. NPs' moving trajectory was observed under different environments (solvent only, with bacteria, with cancer cells) using equipment of NIR introduced fluorescence microscope of (1).

Purpose (3) Informatic analysis: After obtaining movie data of (2), analyze their trajectory using Matlab. Obtaining information processing method: establish Matlab code for (2), analyze the movie data.

Purpose (4) The interaction between bacteria (*E.Coli*)/ cancer cells (MDA-MB-453) and Gd_2O_3:Er,Yb UCNPs (1200℃, 900℃, 900℃-PVP-SiO_2) as a basic research for biomedical application are investigated.

The purpose of this chapter is to confirm NPs behavior in liquid and interaction between cancer cells and various types of UCNPs.

5.2 Experimental

5.2.1 Designing and building up the fluorescence microscope

980 nm laser light source and its laser path including 3 mirrors, 805 nm short pass, the cages, ND filter were designed and built up for fluorescence microscope. Hight of laser path was 2.5 inches. To enter the laser into the microscope correctly, a blue laser was first used for rough laser path adjustment. Subsequently, the 980 nm laser position was adjusted by mirrors (1^{st}: horizontal, 2^{nd}: height, 3^{rd}: minor adjustment) using the detector card (※980 nm laser is not visible). Optics were purchased after design. Constructed NIR induced fluorescence microscope was shown in Fig. 5-1.

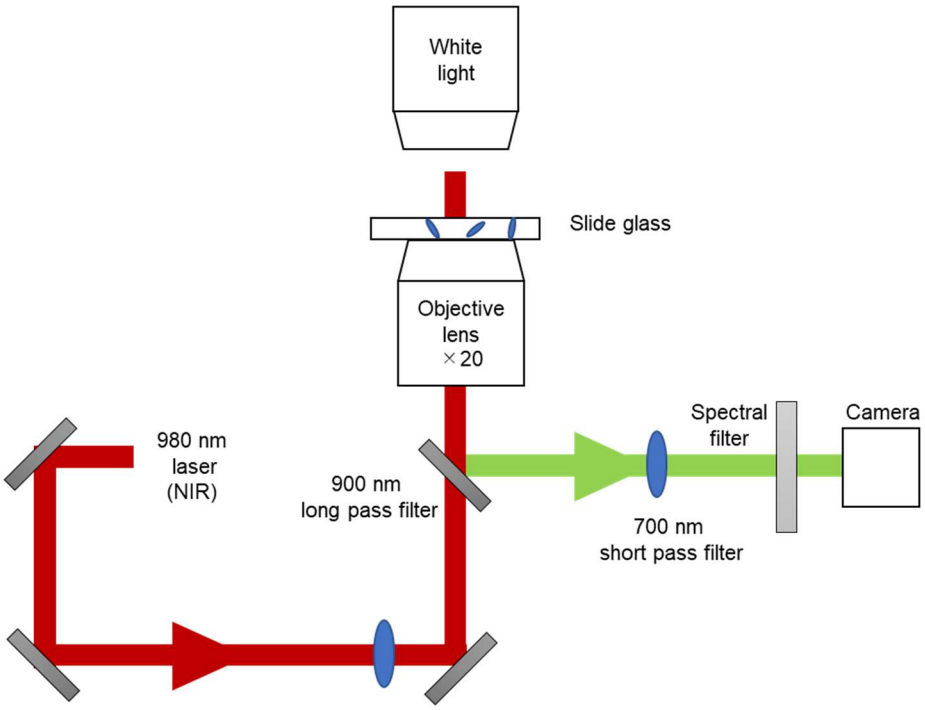

Fig. 5-1 NIR introduced fluorescence microscope.

5.2.2 Observation of NPs movement

(1) Preparation of NPs samples

Used NPs sample were Gd_2O_3:Er,Yb (900℃, 900℃-PVP, 900℃-PVP-SiO_2, 1200℃ (same synthesis method as Chapter 2)), $NaYF_4$:Er,Yb (99%, SIGMA-ALDRICH). Preparation method is summarized in Fig. 5-2.

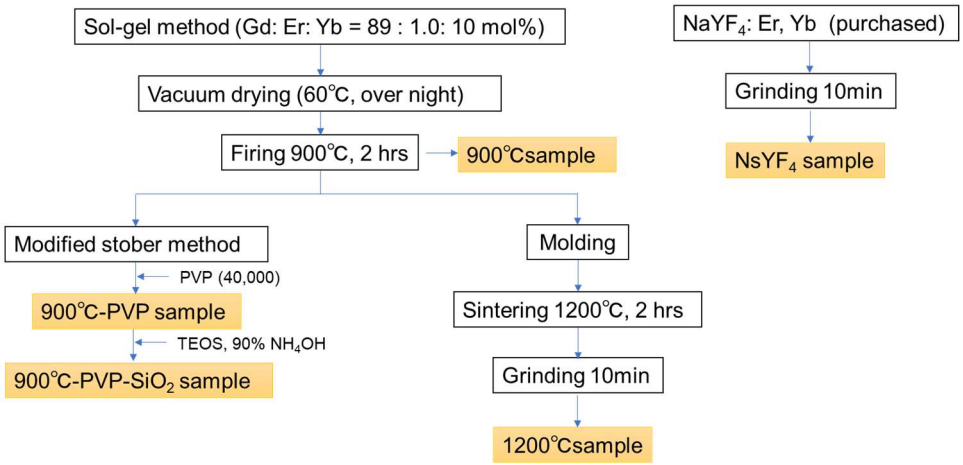

Fig. 5-2 Preparation method of each type of NPs.

0.82×10^{-4} g/mL NPs solution was prepared as follows: 0.011 g powder was added in 1.5

mL tube and 1.1 mL of water was added and mixed well by pipetting 20-30 times (0.01 g/mL NPs solution). Tube was left for 5 min to sediment large particles. 4.1 μL of 0.01 g/mL NPs solution was picked and mixed well in 0.5 mL of water.

(2) Observations of NPs movement

50 μL of 0.82×10^{-4} (g/mL) NPs were dropped to slide glass to observe. The slide glass was covered with another slide glass. NPs movement was observed under the condition of wavelength: 602-660 nm (red emission), exposure time: 25 ms, light source: white light (OFF) and 980 nm NIR, movie data setting: interval 0 ms, 500 frames.

(3) Analysis and calculation by Matlab

Some of the NPs were moving in the water and their movie was obtained. Their trajectory was analyzed in 2 Matlab codes (one is for tracking the movement, and the other one is for calculating the radius and diffusion coefficient). Matlab code for calculating the radius diffusion coefficient was made and calculated.

5.2.3 Interaction between NPs and bacteria

(1) Preparation of bacteria

Bacteria (*E.Coli*) was cultured 2 times.

・Primary culture (1°)：Clean bench and tools were UV sterilization for 20 min. after pouring L. B. media to tubes (1 mL: control, 999 μL: sample), 1-2 μL of original bacteria solution was added into sample tube and well mixed by slow pipetting. The samples were incubated at incubator 12 hours (37℃, 200 rpm).

・Secondary culture (2°)：10 μL of primary cultured bacteria were poured into 10mLof L. B. media in the tube and well mixed by slow pipetting. The sample was incubated at incubator 18 hours (37℃, 200 rpm). In this condition, optical density (OD) was ~0.46.

(2) Mixing 2° bacteria and NPs

50 μL of 2° bacteria and 8.2 μL of 0.01 g/mL NPs were mixed in a tube of 950 μL L. B. media, incubated for 15 min (37℃, 200 rpm).

※NPs type: Gd_2O_3:Er,Yb (900℃, 900℃-PVP, 900℃-PVP-SiO_2, 1200℃ (same synthesis method as Chapter 2))

※0.01 g/mL NPs 950 μL solution preparation: 0.011 g powder was added in 1.5 mL tube and 1.1 mL of L.B. media added and mixed well by pipetting 20-30 times. Tube were left

for 5 min to sediment large particle. Sample solution was picked from middle of tube.

(3) Observation of interactions between NPs and bacteria

50 μL of incubated NPs and 2° bacteria were dropped to slide glass to observe. The slide glass was covered with another slide glass.

Bacterial and NPs were observed under the condition of wavelength: 602-660 nm (red emission), exposure time: 25 ms, light source: white light (ON/OFF) and 980 nm NIR, movie data setting: interval 0 ms, 200 frames.

5.2.4 Interaction between cancer cells and NPs

Provided cancer cell (MDA-MB-453) cultured on slide glass in DMEM liquid and 41 μL of 0.01 g/mL NPs were incubated for 5 hours (37℃). The slide glass was observed by the microscope under the condition of wavelength: 602-660 nm (red emission), light source: white light (ON/OFF), and 980 nm NIR.

※NPs type: Gd_2O_3:Er,Yb (900℃, 900℃-PVP-SiO_2, 1200℃ (same synthesis method as Chapter 2))

※0.01 g/mL NPs 950 μL solution preparation: 0.011 g of powder was added in a 1.5 mL tube and 1.1 mL of L. B. media was added and mixed well by pipetting 20-30 times. The tube was left for 5 min to sediment large particle. Sample solution was picked from the middle of tube.

5.3 Results and discussion

5.3.1 Calculated diffusion coefficient and radius from NPs tracking movie data

Fig. 5-1 shows the calculated diffusion coefficient of each sample derived from movement tracking. Regarding the coating effect between samples of 900℃-PVP-SiO_2, the coating layer increased, wider distribution (low diffusion coefficient). Because of the weight of the layer, the diffusion coefficient became small. Regarding non coated samples (1200℃ and $NaYF_4$:Er,Yb), it showed a similar value.

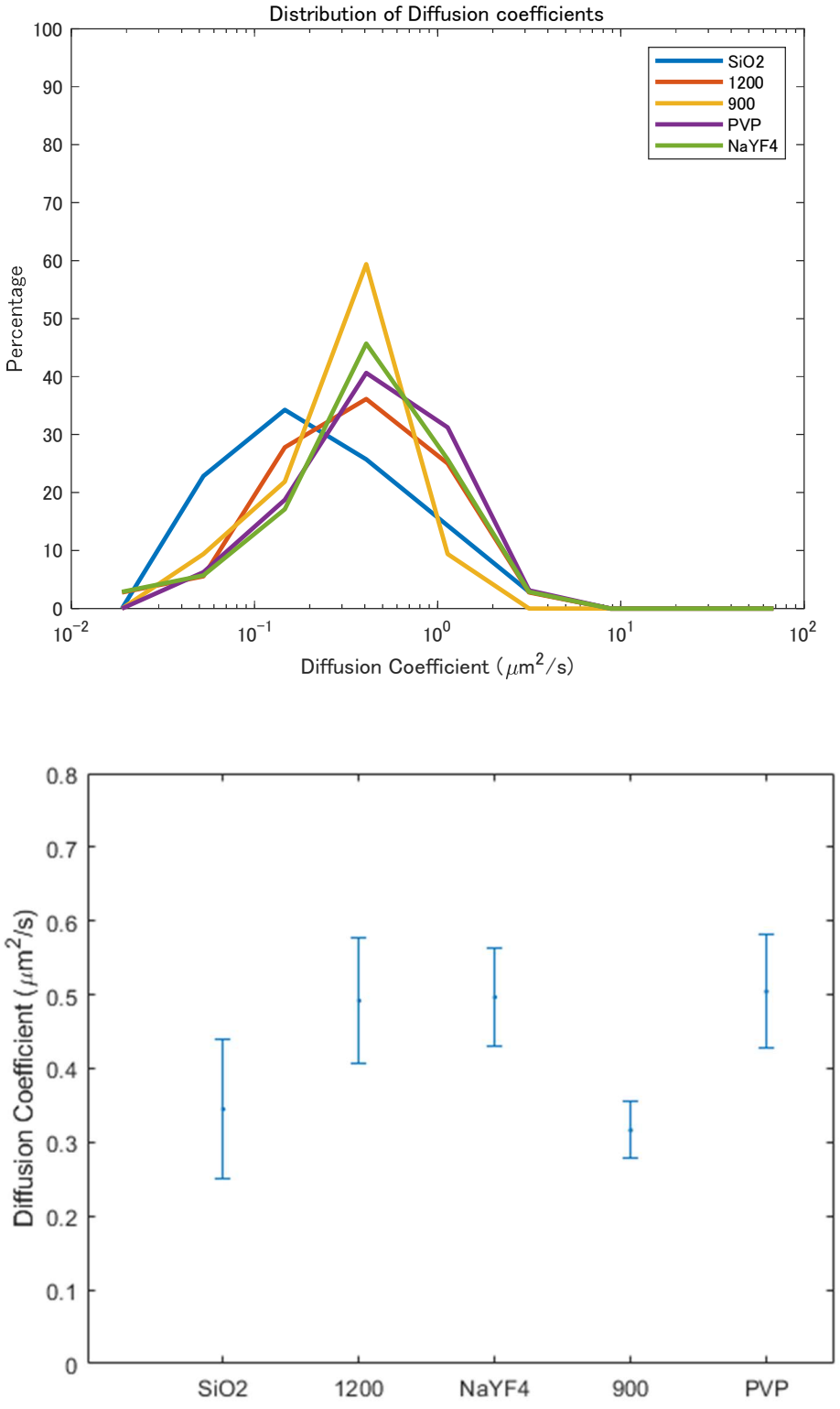

Fig. 5-3 Calculated diffusion coefficient of each sample derived from movement tracking.

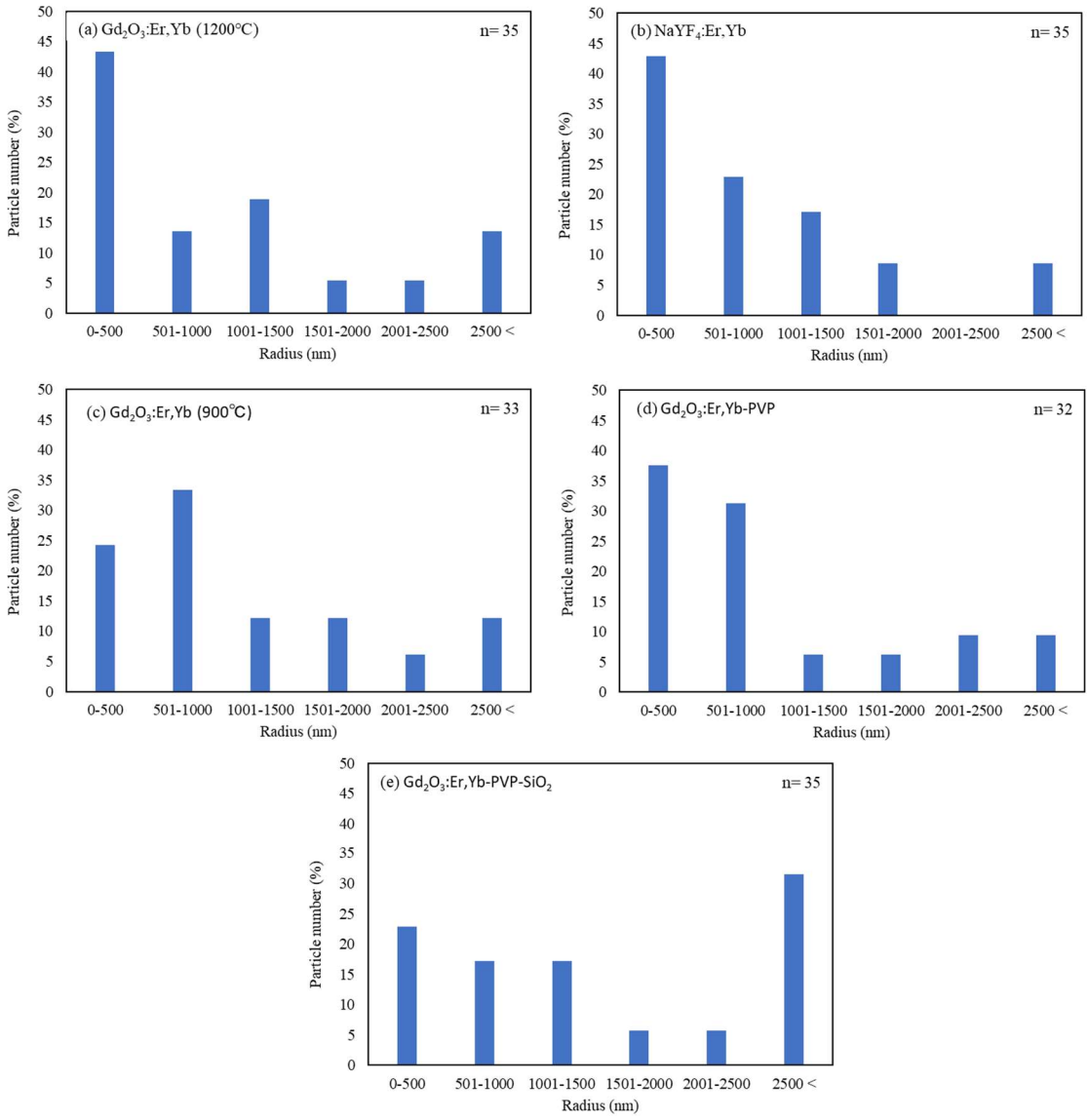

Fig. 5-2 Radius of each sample calculated by diffusion coefficient.

Fig. 5-4 shows the radius of each sample calculated by diffusion coefficient. Frequently observed radius was: < 500 nm as of Fig. 5-4 (a), (b), and (d), 501-1000 nm as of Fig. 5-4 (c), and > 2500 nm as of Fig. 5-4 (e). Theoretically, regarding radius, after 900℃ firing sample is smaller than after 1200℃ sintering sample. Besides, it is said UC emission intensity is strong to $NaYF_4$ > Gd_2O_3 (1200℃) > Gd_2O_3 (900℃) because of their crystal structure. However, the smaller radius of NPs tends to show lower emission from increasing surface detection rate per specific surface area. Therefore, it is considered that the small NPs' emission of 900℃ sample couldn't be found due to their faint emission although it should be the smaller radius of them there.

More precise consideration can be conducted when more experiments. And after processes such as filtering and centrifugation will be helpful to obtain narrow particle distribution. This time, 2D position tracking of phosphors was performed. Applying this to 3D position data, using deep learning and point spread function (PSF) that corrects the blurring of point light sources[5-1], contributes to understanding the movement status of NPs during cell uptake and leads to elucidating the mechanism of biological science.

5.3.2 Interaction between NPs and bacteria

Table. 5-1 Percentage of NPs with bacteria and counted number.

	NPs with bacteria (%) (number)			
Experiment #	1200°C	900°C	PVP	SiO_2
1	27% (56)	23% (75)	11% (74)	50% (28)
2	15% (73)	11% (76)	10% (72)	22% (77)

Table. 5-1 shows the percentage of NPs with bacteria and counted number. To see the difference between the type of NPs and experiment time, Fig. 5-2 was created below.

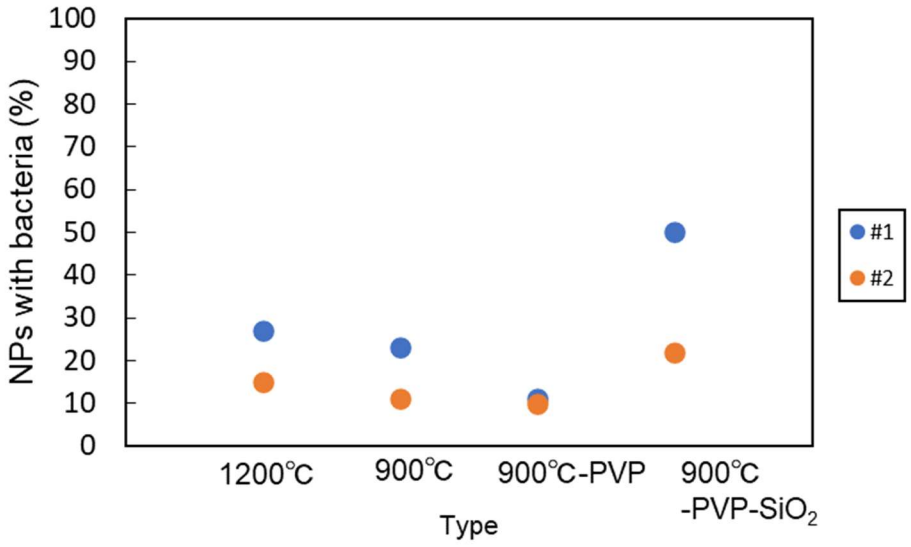

Fig. 5-5 Percentages of NPs with bacteria.

Fig. 5-5 shows percentages of NPs with bacteria results of 2 experiments under the same experimental condition. Between 2 experiments, there was ~ 10% difference except

SiO_2 and ~ 30% difference in SiO_2. However, the overall tendency became similar. SiO_2 had the most attachment to bacteria. PVP is the lowest value. Besides, during observation, after attaching SiO_2 coated NPs, some bacteria still moved, which means bacteria are alive.

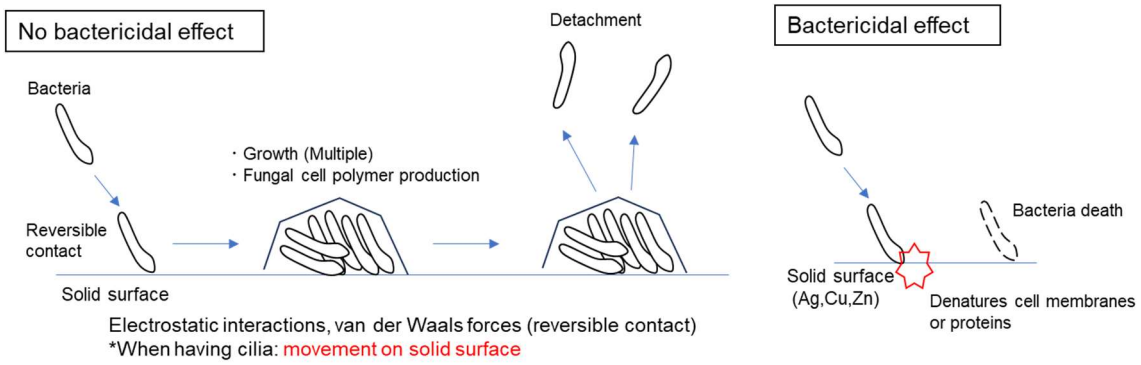

Fig. 5-6 Solid surface and microorganisms attachment scheme.

Fig. 5-6 shows solid surface and microorganism attachment scheme. Microorganisms including bacteria contact solid surfaces due to electrostatic interactions and van der Waals forces between solid (reversible contact). After bacterial contact surface, they can grow on surface. However, if solid surfaces consisted of bactericidal materials such as Ag, Cu, Zn, denatured cell membranes or proteins occur, resulting bacteria death[5-2][5-3].

In this research, *E. coli* has cilia and some of them were moving after they attach NPs. Possibility of no biological toxicity especially SiO_2 sample. Therefore, this result implies SiO_2 coated NPs tend to stick easily because of their biocompatibility and do not kill the bacteria (not toxic to microbial).

5.3.3 Interaction between NPs and cancer cells

Table. 5-2 Percentage of cancer cells with NPs and counted number.

Type of NPs	Fraction of cell with NPs (%)	Counted number of cells
Gd_2O_3:Er, Yb (1200°C)	77.3	203
Gd_2O_3:Er, Yb (900°C)	56.9	195
Gd_2O_3:Er, Yb (900°C)-PVP-SiO_2	60.8	176

Table. 5-2 shows the percentage of cancer cells with NPs and counted number. From Table. 5-2, the highest percentage which have NPs were 1200°C NPs' ~77%. And 900°C and SiO_2 coated samples were ~ 60 %. From these results, there is a possibility that NPs

tend to attach cancer cells regardless of NPs type. However, to know more precise tendency, multiple time experiments (at least 3 times) under same conditions are needed.

NPs uptaking into cancer cells is the most important to apply PDT because after that, aimed PDT with UCNPs can be started. After attaching cancer cells and NPs, the experiment of uptaking of NPs can be conducted. Thus, these experiments became the first step for them.

5.4 Summary

NIR induced fluorescence microscope was designed and assembled. Using this equipment, behavior of various NPs was tracked and analyzed. The diffusion coefficient and particle size were calculated using the created Matlab code. Interaction between each NPs and bacteria/cancer cells were investigated. Bacteria had a high rate of adhesion to the SiO_2 coated NPs and remained movement even after adhesion, suggesting that the NPs are not toxic. Investigation of interactions with cancer cells suggested high adhesion. It is desirable that these experiments repeated multiple times (at least 3 times) under the same conditions.

5.5 References

[5-1] P. Zelger, K. Kaser, B. Rossboth, L. Velas, G. J. Schütz, and A. Jesacher, Opt. Express, 26, (2018), 33166.

[5-2] T. Tsuchido, es, 31, (2003), 5.

[5-3] T. Ishida, Materiaru Raifu Gakkaishi, 23, (2011), 21.

Chapter 6
General conclusions and perspectives

6.1 General conclusions

As shown in Table. 1-1, 4 tasks of UCNPs for PDT application were investigated throughout this thesis. The tasks and obtained results are summarized below.

(Task 1) Excitation & emission range: It needs excitation at 980 nm NIR light and emission of visible light (400-800 nm). To solve this, optimal dopant ion selection is needed. This time, Yb ion (sensitizer) and Er ion (activator) were selected.
(Result 1) From PL results, the irradiated NIR was successfully converted to visible light especially peaks of around 410 (blue), 560 (green), and 660 nm (red) which is specific to Er. Adding this to TEM-EDS and XRD results, it is considered that Er and Yb was doped in the host matrix (Gd_2O_3).

(Task 2) Emission intensity: Upconverted visible light should have efficient light intensity at the corresponding wavelength of the photosensitizer's absorption area. It should have enough intensity to activate them. The strongest light emission area varied by changing the matrix. This time, Gd_2O_3 was selected for strong red light emission.
(Result 2) From the PL result, the strongest red emission was obtained which corresponds to strong absorption of photosensitizer Ce6 by selecting the host matrix as Gd_2O_3. From the ROS occurrence test result at cuvette scale, ROS was successfully generated which was the result of activated photosensitizer Ce6 by Gd_2O_3:Er,Yb UCNP's red light. Thus, the UCNPs have enough emission intensity for aimed PDT with UCNPs reaction scheme.

(Task 3) Particle size: Since the UC phenomenon is needed in the cancer cell, it is needed to make them miniaturization (10-200 nm). Also, light emission intensity from phosphor depends on crystallinity, it is needed to maintain its crystallinity when miniaturization. To solve this, laser ablation in liquid (LAL) is optimal.
(Result 3) From XRD result, the raw material was miniaturized while its crystal structure was maintained. At low fluence, coarse NPs (d> 200 nm) were obtained, and from middle fluence fine NPs (< 100 nm) were started to generate. At high fluence, fine NPs increased. Fine NPs had smaller diameters than that of raw materials, therefore LAL occurred and fine NPs were generated. Adding to it, regarding laser irradiation time, after 15 min irradiation, the primary particle size distribution became similar. From these results, to obtain 10-200 nm sized NPs by LAL, the appropriate condition was 8.9 J/cm^2 and >15 min laser irradiation time. However, since the laser is a Gaussian beam, particle size distribution occurs even if it is at high fluence. To make it narrow particle size distribution which is needed PDT, centrifugation (5000rpm × 20 min) and ~ 2 mL from the top were

effective. Besides, fine NPs have particular properties such as easy aggregation and photon number increase when they become < 100 nm. For countermeasures for these, surface coating is effectiv.

(Task 4) Biocompatibility: To prevent elimination by body as foreign matter after installation, surface coating around UCNPs with high biocompatibility material is needed. (Result 4) NPs were successfully surface coated by PEG, PVP, and SiO_2. PEG coated NPs showed PL intensity increase compared to non-surface coating ones. Adhesion with bacteria and cancer cells was confirmed. Especially, some bacteria had movement after they were attached to SiO_2 coated NPs. This implies SiO_2 coated NPs have no toxicity to microbial.

6.2 Perspectives

Regarding experimental aspect, as ROS occurrence test, optimization (concentration of Ce6, UCNPs) is needed to achieve weak NIR laser input for PDT clinical application. By investigating quantum efficiency (light emission per particle), the relationship between particle size and emission intensity for more deep consideration can be obtained. As a microbial experiment, NPs uptake in cancer cells and cell viability by MTT assay is needed. After that, confirmation of PDT with UCNPs reaction scheme in cancer cells is also needed for the first step of the actual application process.

As for the impact on society, in Japan, which is facing an aging society, there is a need for non-invasive cancer treatment methods that pursue the quality of life of patients. Heavy ion radiotherapy, which is one of non-invasive cancer treatment, requires large equipment and a lot of energy to create high-speed carbon beams. However, since the treatment method of PDT with UCNPs does not require large equipment or energy, it realizes a social design that contributes to a zero-carbon energy society. UCNP also expands the range of PDT treatment, which can help many patients.

There are many aspects of the uptake mechanism into cells that have not yet been elucidated. However, by using information science to elucidate 3D position data measured with a fluorescence microscope, new laws regarding drug delivery can be discovered, and the development of medical science using information science can be expected.

Acknowledgments

This study was performed under the guidance by Associate Professor Hiroyuki Wada in Tokyo Institute of Technology. I deeply appreciate Associate Professor Hiroyuki Wada for his persistent support, wonderful guidance, and great advice with my greatest appreciation.

This work was supported by Japan Science and Technology Agency Support for Pioneering Research Initiated by the Next Generation (JST SPRING), Grant Number JPMJSP2106 and Tokyo Tech Academy of Energy and Informatics.

I would like to express my sincere gratitude Professor Yoshitaka Kitamoto for SEM analysis, Professor Masahiko Hara for DLS measurement in Tokyo Institute of Technology.

I would like to express my great gratitude to Ms. K. Suda for XRD analysis and Ms. Y. Akimoto for TEM-ESD analysis in Open Facility Center, Materials Analysis Division, Tokyo Institute of Technology.

I sincerely appreciate all of the people who have greatly supported me and cooperated with me for a long time including my seniors, colleagues, juniors in Wada laboratory, many professors, mentor of Tokyo Tech Academy of Energy and Informatics, many staff of Tokyo Tech, people who related research internship, many friends, family, relatives and partner.